RESULTS AND DISCUSSIONS

1. Adsorption of ethylene, benzene, and ethylbenzene over faujasite zeolites investigated by the ONIOM method

1.1 Models of faujasite catalyst

The cluster models were taken from the lattice structure of faujasite zeolite. The 3T cluster $H_3SiOAl(OH)_2O(H)SiH_3$ (Figure 13) is considered as the smallest unit required to represent the active site of zeolite. One of the silicon atoms in faujasite zeolites is substituted by an aluminum atom, and a proton is added to one of the oxygen atoms bonded directly to the aluminum atom. Then, the larger clusters were proposed for representing the system of protonated faujasite (H-FAU). The 20T model, illustrated in Figure 14, is the 12-membered-ring window connecting two supercages of faujasite, including eight more tetrahedral atoms at the base next to the Al atom. The largest 84T cluster, including two supercages, acts as a nanoscopic reaction vessel (Figure 15) where the adsorbates can be trapped inside. Due to the limitation of computational resources and time consumption, the active region is treated more accurately with the ab initio method, while interaction in the rest of the model is approximated by a less accurate method.

According to the two-layer ONIOM approach, the calculation of energies can be simplified by treating the active region (i.e., the active Brønsted acidic site of a zeolite catalyst) with a high-level quantum mechanical (ab initio or density functional) approach, and the extended framework environment with a less expensive level, the HF, semiempirical, and molecular mechanics force fields methods. The total energy of the whole system can be expressed within the framework of the ONIOM methodology developed by Morokuma and co-workers, where the superscript Real means the whole system and the superscript Cluster means the active region, which would be treated with the higher level of calculation. Subscripts High and Low mean high- and low-level methodologies used in the ONIOM calculation. In this study, the high-level region is treated by the Hartree–Fock and the density functional theory

with the hybrid functional B3LYP. The remainder is treated by molecular mechanics force fields (Rappe *et al*., 1992), semiempirical or the Hartree–Fock methods.

The accuracy of the QM/MM method, particularly the ONIOM method, depends significantly on the choice of the level of calculations for high- and low-level regions. Progressing through various types of quantum mechanics, semiempirical, and molecular mechanics methods, the experimental adsorption energy of the benzene/zeolite system can be used to validate the choice of methods. Using the B3LYP method for treating the quantum cluster, the methods for the low-level region from the molecular mechanics force fields (UFF), semiempirical, over to the Hartree–Fock methods were varied. Using the experimental observation as a benchmark, the UFF method is found to provide reasonable values corresponding to the experimental prediction. This is due to the explicit consideration of van der Waals contribution, which is the dominant contribution in adsorptiondesorption in zeolites. Therefore, the UFF method is the practical choice for the low-level methodology when the high-level region is treated by the B3LYP/6-31G(d,p) method.

All calculations in this part have been performed by using Gaussian98 code (Frisch *et al*., 1998). The basis set for the Hartree–Fock calculations is 3-21G, while the basis set 6-31G(d,p) is utilized for the B3LYP calculations. During the structure optimization, only the active site region, [≡SiO(H)Al(O)$_2$OSi≡], and the adsorbate are allowed to relax.

In order to obtain more reliable interaction energies, basis sets superposition error (BSSE) corrections were also taken into account. In addition, the common practice of running a higher level single-point energy calculation at the geometry generated by use of a cheaper method is as effective as performing all calculations at the higher level of theory. Thus, using the optimized geometries produced by the B3LYP/6-31G(d,p), the single-point energy calculations at the B3LYP/6-311++G(d,p) level are carried out.

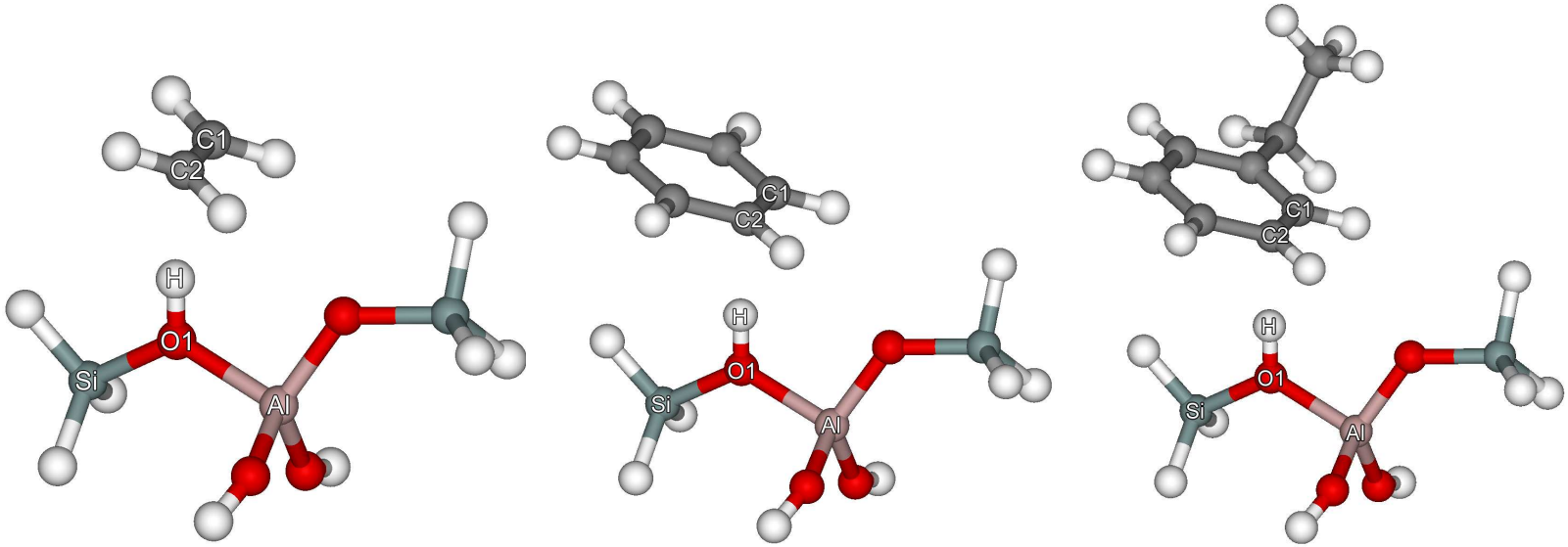

(a) (b) (c)

Figure 13 Presentation of models of faujasite and interacting with adsorbates: a) full 3T cluster model interacting with ethylene; b) full 3T cluster model interacting with benzene; and c) full 3T cluster model interacting with ethylbenzene.

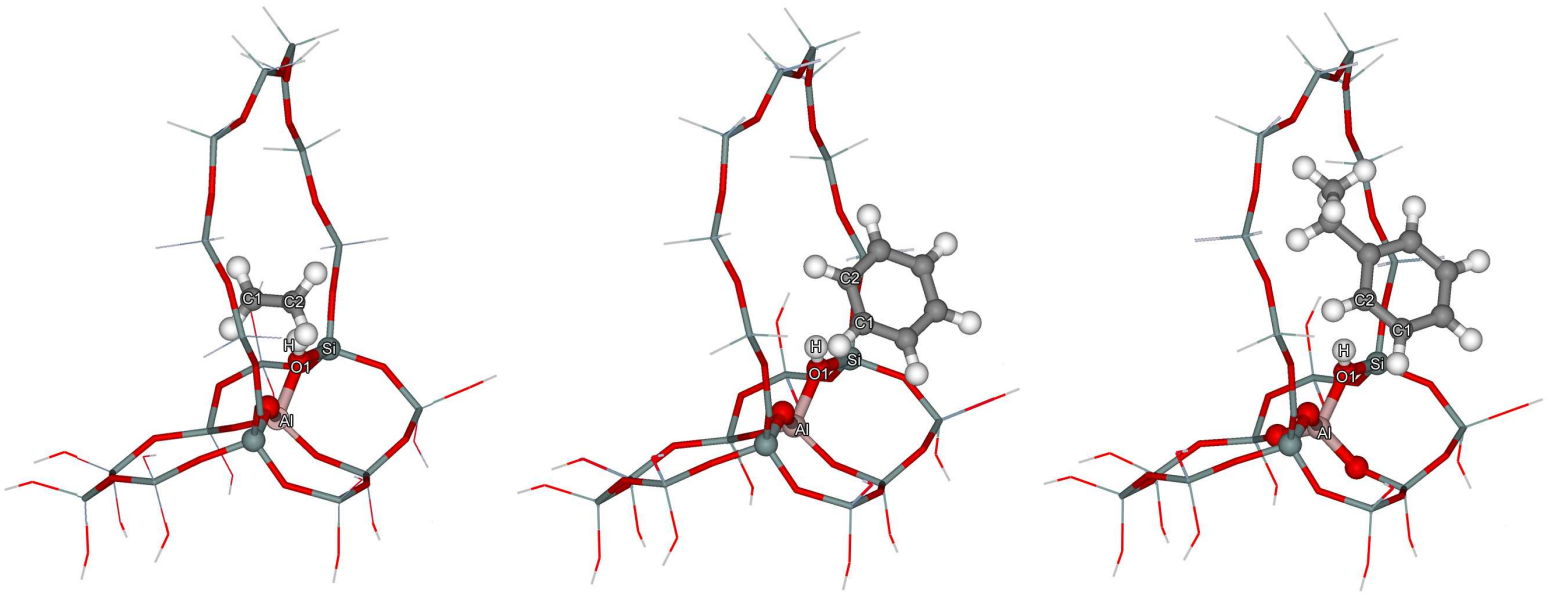

(a) (b) (c)

Figure 14 Presentation of models of faujasite and interacting with adsorbates: a) ONIOM2 layer models of 20T cluster interacting with ethylene; b) ONIOM2 layer models of 20T cluster interacting with benzene; and c) ONIOM2 layer models of 20T cluster interacting with ethylbenzene. Atoms belonging to the high level regions are drawn as spheres.

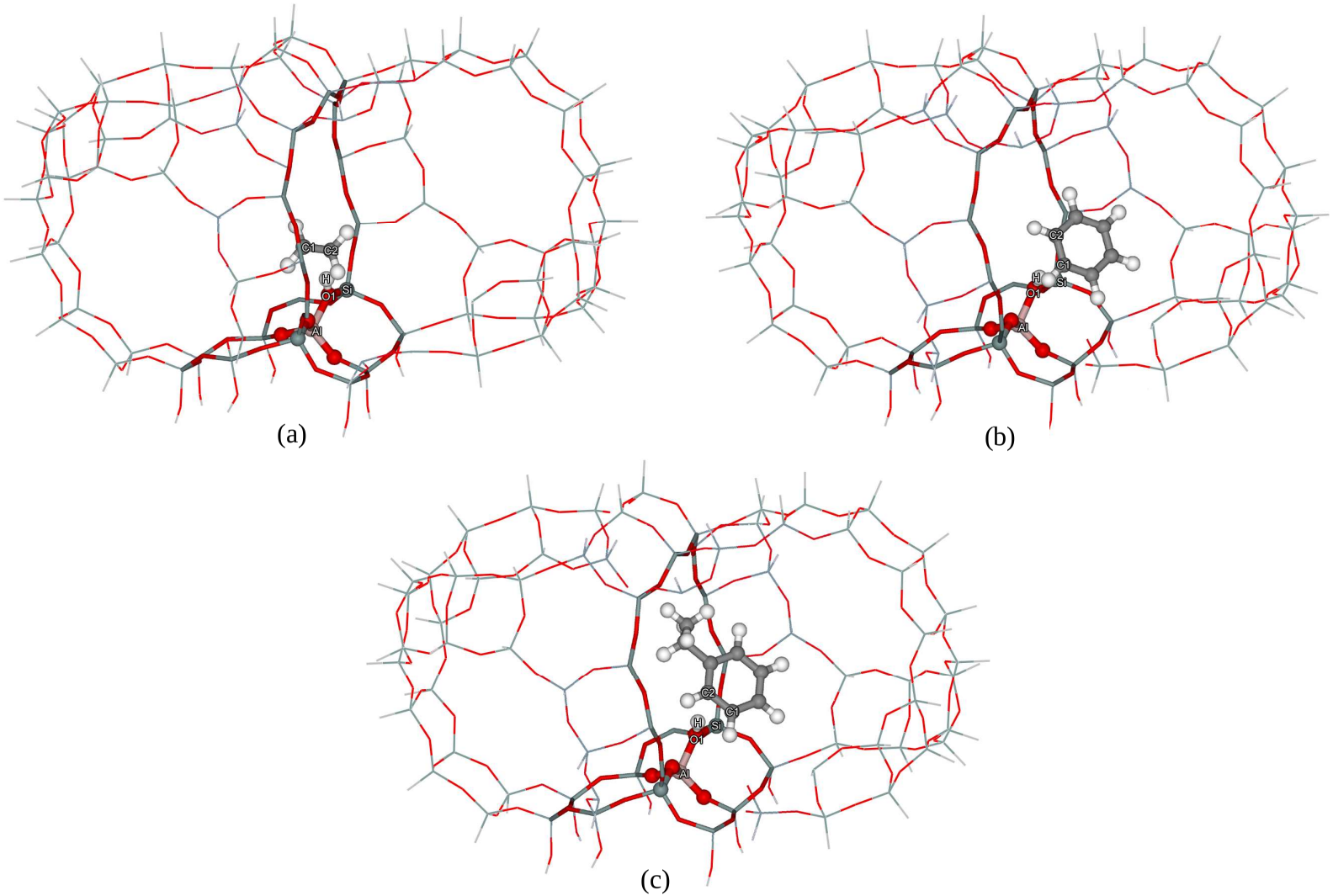

Figure 15 Presentation of models of faujasite and interacting with adsorbates: a) ONIOM2 layer models of 84T cluster interacting with ethylene; b) ONIOM2 layer models of 84T cluster interacting with benzene; and c) ONIOM2 layer models of 84T cluster interacting with ethylbenzene. Atoms belonging to the high level regions are drawn as spheres.

Table 1 Binding energy of ethylene, benzene and ethylbenzene on the Brønsted proton of faujasite zeolites (binding energy in kcal/mol).

Methods/Models	3T			20T			84T		
	ethylene	benzene	ethylbenzene	ethylene	benzene	ethylbenzene	ethylene	benzene	ethylbenzene
B3LYP/6-31G(d,p)	-8.14	-7.48	-7.76	-10.93[a]	-14.28[a]	-15.90[a]	-	-	-
B3LYP/6-31G(d,p):UFF	-	-	-	-10.78	-14.94	-18.35	-11.49	-17.15	-22.99
B3LYP/6-31G(d,p)+BSSE[d]	-7.61	-6.54	-6.69	-10.25	-13.93	-17.30	-10.96	-16.15	-21.94
B3LYP/6-311++G(d,p)[b]	-5.39	-5.35	-5.78	-8.03	-12.23	-16.40	**-8.75**	**-15.17**	**-21.08**
HF/3-21G	-8.37	-9.49	-9.88	-10.90	-13.16	-17.23	-	-	-
HF/3-21G:UFF	-	-	-	-10.48	-16.76	-19.73	-11.43	-18.33	-24.09
HF/3-21G+BSSE[d]	-7.85	-8.42	-8.29	-10.05	-15.74	-18.50	-10.91	-17.21	-22.84
HF/6-311++G(d,p)[c]	-3.28	-3.47	-3.91	-6.21	-10.51	-11.74	-6.54	-13.69	-19.65
B3LYP/6-31G(d,p):HF/3-21G	-	-	-	-10.98	-11.40	-12.00	-	-	-
B3LYP/6-31G(d,p):MNDO	-	-	-	-6.99	-3.37	-3.23	-	-	-
B3LYP/6-31G(d,p):AM1	-	-	-	-7.67	-4.49	-4.99	-	-	-
B3LYP/6-31G(d,p):PM3	-	-	-	-5.41	-1.95	-1.13	-	-	-
HF/3-21G:MNDO	-	-	-	-7.10	-5.67	-5.65	-	-	-
HF/3-21G:AM1	-	-	-	-7.34	-6.50	-7.25	-	-	-
HF/3-21G:PM3	-	-	-	-5.63	-4.31	-4.12	-	-	-

Experimental adsorption energies of ethylene on H-FAU is -9.1 kcal/mol, taken from cant and Hall (1972)

Experimental adsorption energies of benzene and ethylbenzene on H-FAU are -15.3 kcal/mol and –19.6 kcal/mol, repectively, taken from (coker *et al*., 2000)

[a]Mixed basis sets of 6-31G(d,p) and 3-21G. [b]Indicates single point energy at indicated level of theory on the optimized B3LYP/6-31G(d,p): UFF structure.

[c]Indicates single point energy at indicated level of theory on optimized HF/3-21G: UFF structure and [d] Basis set superposition error corrected

1.2 Adsorptions of ethylene, benzene, and ethylbenzene with models of faujasite zeolites

The adsorption energy is one of the most valuable data obtained from experimental observation which can be used to validate the theoretical data. The adsorption energies of ethylene, benzene, and ethylbenzene on H-FAU zeolites calculated from different models, and also those from the ONIOM models using the semiempirical and molecular mechanics force fields for the outer layer are presented in Table 1. Using the 3T cluster model, the DFT methods predict the adsorption energies of ethylene, benzene, and ethylbenzene to be −8.14, −7.48, and −7.76 kcal/mol, respectively. This is in contradiction with the experimental results. The adsorption energy of ethylene on the acidic H-FAU zeolite was determined to be −9.1 kcal/mol (Cant and Hall, 1972). The adsorption energies of benzene and ethylbenzene on H-FAU zeolites were experimentally measured to be −15.3 ± 1 and −19.6 ± 1 kcal/mol, respectively, indicating that the enthalpy of adsorption (ΔH_{ads}) of benzene is less than that of ethylbenzene (Coker *et al*., 2000).

Increasing the cluster size from 3T to 20T clusters, the calculated adsorption energies (ΔE_{ads}) of ethylene, benzene, and ethylbenzene interacted with zeolites are well differentiated (Table 1). Tests on the 20T clusters show that the ONIOM2 schemes, only the ONIOM2(B3LYP/6-31G(d,p):UFF) but not other ONIOM2 schemes, can be compared favorably with the full HF and B3LYP levels of theory. Using semiempirical methods, i.e., AM1, PM3, and MNDO for the outer layer, the wrong trend of ΔE_{ads} is observed as compared to the experimental data. The ONIOM2 model can substantially reduce the computational expense. For example, the single-point calculation of the 20T/ethylene complex on an SGI machine (Origin 200) requires about 5 min (computational time) for the ONIOM2(B3LYP:UFF) method whereas, the full quantum cluster requires more than 50 min. This again confirms that the cost-effective ONIOM2 strategy should be utilized to obtain an accurate description of the system. Increasing the cluster size from 20T up to the more realistic model, 84T, by enlarging the outer layer, the differences between each adsorption energy are pronounced. The adsorption energies of ethylene, benzene, and

ethylbenzene calculated from the 84T cluster using ONIOM2 (B3LYP/6-31G(d,p):UFF) are calculated to be −11.49, −17.15, and −22.99 kcal/mol, respectively. These interaction energies are somewhat overestimated as compared to the experimental results. Including the basis set correction by single-point calculations at the higher basis set, 6-311++G(d,p), the corresponding interaction energies are predicted to be of −8.75, −15.17, and −21.08 kcal/mol. The BSSE corrections were also performed and gave similar results as the single-point calculations at the high basis set (see Table 1). These results are in good agreement with the experiment (Cant and Hall, 1972, Coker *et al*., 2000). However, one may question if the energy could change if the model becomes bigger and bigger. To ensure the convergence of the ONIOM model, the structure optimization of a larger model of 336T with ethylbenzene has been carried out at the HF:UFF level of calculation. The adsorption energy of −24.60 kcal/mol from the 336T model is almost identical to the 24.09 kcal/mol from the 84T model at the same level of calculation, indicating that the use of the 84T ONIOM model is practical and increasing the model size would not have any profound effect on the energetics of the system.

It is noted that the choices of the methods using the high and low-levels in the ONIOM scheme and also the sizes of the inner and outer regions are arbitrary. The size of the inner region employed in this study (3T cluster) is sufficient to represent the acid property of zeolites while small enough to guarantee that the van der Waals interactions between the hydrocarbon and the zeolite are well accounted for by the UFF force field, which is better than the DFT for this purpose (Vos *et al*., 2001, Rozanska *et al*., 2001, Clark *et al*., 2003). Using the larger inner region, which may require the use of theMP2 level of theory in place of DFT, will be advantageous in searching for the transition state leading from ethylene and benzene to ethylbenzene. This challenging reaction is being actively pursued. From the structure and adsorption energy point of views, the B3LYP combining the UFF force fields method as a lower level is considered to be one of the best combinations for the ONIOM2 scheme. This efficient scheme provides a cost-effective computational strategy for treating the effects of a large extended framework structure.

2. Alkylation of benzene with ethylene and dimerization of ethylene

The van der Waals interactions between hydrocarbon as well as aromatic adsorbates and the zeolite wall contribute significantly to the energetic of the adsorption–desorption process in zeolites (Bobuatong *et al.,* 2003, Clark *et al.,* 2003, Derouane *et al.,* 2000, Kasuriya *et al.,* 2003, Olson *et al.,* 1969, Panjan *et al.,* 2003, Pelmenschikov *et al.,* 1999, Raksakoon *et al.,* 2003, Rozanska *et al.,* 2001, Vos *et al.,* 2001, Wesolowski *et al.,* 1997). Besides, typical small quantum cluster calculations which basically neglect these interactions result in erroneous adsorption energies. On the other hand, the hybrid methods such as QM/MM and ONIOM can reasonably describe the interactions with the zeolite framework and have been reported to give adsorption energies close to experimental values (Bobuatong *et al.,* 2003, Kasuriya *et al.,* 2003, Panjan *et al.,* 2003, Raksakoon *et al.,* 2003). Therefore, in this thesis project, the ONIOM method is selected to investigate the interesting reactions catalyzed by zeolites.

2.1 Model of faujasite catalyst

In this part, the 84T of faujasite model in Figure 10 is selected to investigate the reaction mechanism of alkylation of benzene with ethylene. Table 2 shows the selected structural parameters of faujasite model. The structure of the active site obtained from the 3-layered ONIOM model is in reasonable agreement with the structure obtained the 20T full quantum cluster optimized at B3LYP/6-31G(d,p) level theory (see Table 1). The Brønsted O1–H1 and Al–O1 and Si1–O1 bond distances are very close to the values reported in the 20T full quantum cluster (Kasuriya *et al.,* 2003). Further support for the reliability of the active site subunit, ≡ $SiO(H)Al(O)_2OSi$≡, is given from the NMR measurements that the internuclear distance between the aluminum and proton nuclei in a Brønsted acid site, r(Al···H), of faujasite which is reported to be 2.38 ± 0.04 Å (Freude *et al.,* 1988) and, more recently, 2.48 ± 0.04 Å (Hill *et al.,* 1999) and our computed r(Al···H) is 2.462 Å, which is reasonably close to the experimentally measured value.

2.2 Adsorption adsobate molecules on the Brønsted acid site

Ethylene weakly adsorbs onto the zeolite acid site via π-interaction. The weak interaction does not significantly perturb the structure of ethylene and the zeolite. Upon the adsorption of ethylene, only minor changes of the zeolite structure were detected (less than 0.03 Å and 2° for changes in bond distances and bond angles, respectively). Nevertheless, the C–C double bond distance of the ethylene molecule is increased slightly from 1.335 to 1.344 Å and the acidic O1–H1 bond distance is increased from 0.970 to 0.996 Å, indicating that the adsorption slightly weakens the C–C double bond and the acidic O1–H1 bond, which may lead to the protonation of ethylene and the formation of the alkoxide intermediate. The adsorption energy is computed to be −8.73 kcal/mol, which compared well with the experimental observation of −9.0 kcal/mol (Cant *et al.*, 1972).

Benzene and ethylbenzene also weakly interact with the zeolite acid site via π-interaction. The C–C double bond in the benzene ring that forms the π-interaction with the zeolite is slightly increased and the acidic O1–H1 bond distance is slightly increased from 0.970 to 0.985 Å for both benzene and ethylbenzene adsorption complexes, respectively. Similar to the adsorption of ethylene, the zeolite structural parameters are slightly changed by the weak interactions (changes in bond distances and bond angles are less than 0.02 Å, and 2°, respectively). Obviously, the van der Waals interaction for the case of benzene is weaker than for the ethylbenzene adsorption and, hence, the corresponding adsorption energies are −13.91 and −20.11 kcal/mol for benzene and ethylbenzene, respectively. These values are very close to the experimental values of −14.0 (Barthomeuf *et al.*, 1973) and −20.4 kcal/mol (Ruthven *et al.*, 1986) for adsorption of benzene and ethylbenzene in H–Y zeolites, respectively. The accurately predicted adsorption energies clearly demonstrate that the ONIOM3 model used in this work can represent interactions between the adsorbates and zeolite very well. The combination of the MP2 method at the active region embedded in the extended structure modeled by the HF and UFF methods apparently works well in representing electron correlation, electrostatic, and van der Waals interactions in the zeolite system.

2.3 Reaction mechanisms for alkylation of benzene with ethylene and dimerization of ethylene

The reaction mechanisms of both reactions are considered to occur either by a concerted mechanism or by a stepwise mechanism through the formation of an alkoxide intermediate.

A. Stepwise mechanism

A.1 First step (Alkoxide intermediate formation)

The stepwise reactions of both and alkylation of benzene with ethylene and dimerization of ethylene are started with the same first step of reaction called the alkoxide intermediate formation which can be viewed to proceed according to following steps:

$$C_2H_4 + H\text{–}FAU \rightleftharpoons C_2H_4\text{–}H\text{–}FAU \quad \text{(eq.1)}$$

$$C_2H_4\text{–}H\text{–}FAU \rightleftharpoons CH_3CH_2\text{–}FAU \quad \text{(eq.2)}$$

Step (1) is the adsorption of ethylene on the acid site of the zeolite. Then, in step (2), protonation of the adsorbed ethylene occurs, leading to the formation of an alkoxide intermediate.

Table 2 The optimized geometric parameters of isolated zeolite clusters (20T and ONIOM model), ethylene adsorption complex, transition state (TS1), and alkoxide intermediate of steps (1) and (2) on FAU using ONIOM3 (distances are in angstroms and angles are in degrees).

Parameters	20T Full DFT [a]	Isolated cluster	Ethylene adsorption	TS1	Alkoxide intermediate
Distances					
Al-H1	2.508	2.462	2.471	2.655	-
C1-C2	-	1.335	1.344	1.397	1.502
C1-H1	-	-	2.048	1.204	1.084
C2-H1	-	-	2.119	-	-
O1-H1	0.969	0.970	0.996	1.462	-
C2-O2	-	-	-	2.223	1.521
Al-O1	1.914	1.876	1.856	1.755	1.698
Al-O2	1.700	1.694	1.699	1.773	1.878
Si1-O1	1.704	1.669	1.658	1.614	1.595
Si2-O2	1.608	1.606	1.601	1.625	1.681
Angles					
∠Si1O1Al	128.4	123.7	123.5	122.0	118.1
∠Si2O2Al	129.9	130.4	131.8	132.9	132.8

[a] Kasuriya *et al*., 2003

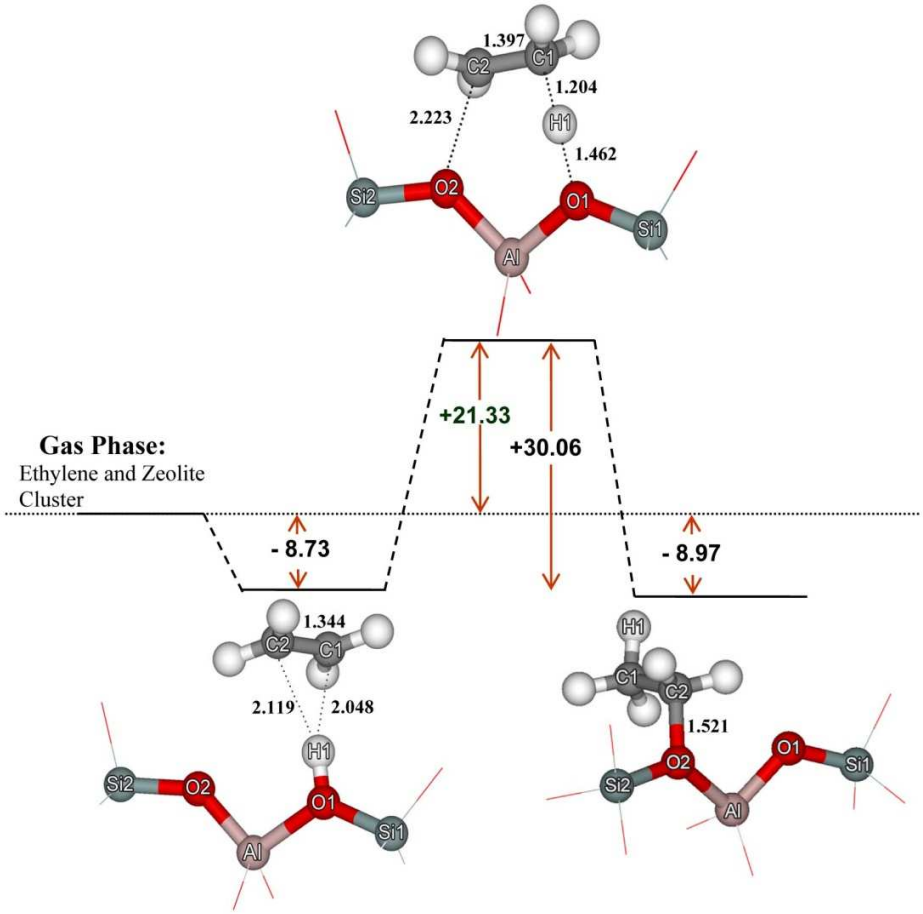

a)

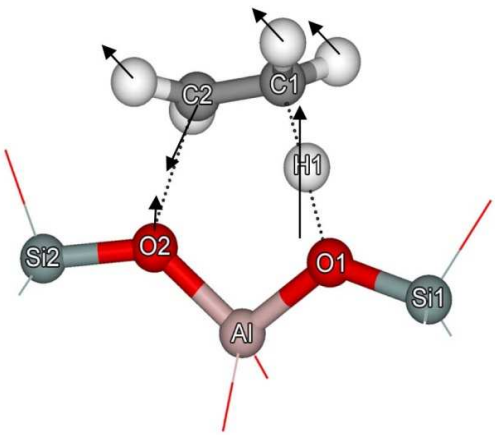

b)

Figure 16 (a) Calculated energy profile for the stepwise reactions in steps (1) and (2) of benzene alkylation and dimerization of ethylene. (b) Vibrational movement corresponding to the imaginary frequency at the transition structure of step (2).

Figure 16a shows the calculated energy profile for the reactions in steps (1) and (2) and Table 2 shows selected geometric parameters of the intermediates and transition state. Ethylene weakly adsorbs on the acid site via π-interaction with the adsorption energy of −8.73 kcal/mol. The weakly adsorbed ethylene can be protonated by the acidic proton. The protonated ethylene is, however, not stable in a form of carbenium ion and, hence, it is quickly transformed to a stabilized alkoxide intermediate by forming a covalent bond to one of the bridging oxygen atoms. At the transition state (Figure 16b) there is one imaginary frequency at 619 cm^{-1} corresponding to the following movements: the zeolite proton is moving toward a carbon atom of the ethylene while the C–C double bond of the ethylene is elongated from 1.344 to 1.397 Å and the other carbon atom is moving toward the adjacent oxygen atom of the zeolite framework to form a covalent bond.

The energy barrier for the protonation is calculated to be 30.06 kcal/mol and the apparent activation energy for this step is 21.33 kcal/mol. The computed apparent activation energy is in reasonable agreement with the estimated range of apparent activation energy for the isotope exchange of ethylene in zeolites of 15–20 kcal/mol reported in the literature (Cant *et al.*, 1972, Evleth *et al.*, 1996). The formation of the covalent bonded ethoxide species is accompanied by significant structural changes of the zeolite. The Al–O1 and Si1–O1 bond distances are decreased by 0.178 and 0.074 Å, respectively, as the Si1–O1–Al bond angle is decreased by 5.6°. While, the Al–O2 and Si2–O2 bond distances are increased by 0.184 and 0.075 Å, respectively, as the Si1–O2–Al bond angle is increased by 2.4° (Table 1). Rozanska *et al*. (Rozanska *et al.*, 2002) have shown that when the zeolite framework is modeled by an unrealistic constraint model, erroneous results can be obtained.

In the ONIOM model, the small cluster of the active region is generally connected to the outer layer of the system via fixed anchoring atoms. Therefore, only a number of atoms at the active site region can be relaxed. In our model, although only atoms belonging to the active site region [$\equiv SiO(H)Al(O)_2OSi \equiv$] are allowed to relax, the energetic properties of the system, e.g., adsorption energies, and activation energy for ethylene protonation, are reasonable and compared

well with previously reported values by experimental measurements and theoretical calculations (Barthomeuf *et al.,* 1973, Cant *et al.,* 1972, Ruthven *et al.,* 1986), indicating the validity of the model. It has been shown that the stability of alkoxide intermediates formed in the zeolite structure is very sensitive to the local geometry of the active site (Boronat *et al.,* 2001).

When the geometry of the system is modeled to represent a particular zeolite structure, the covalent bond between the alkoxide species and the zeolite is weakened and the alkoxide is greatly destabilized due to the steric constraints of the zeolite pore walls (Boronat *et al.,* 2001, Rozanska *et al.,* 2002). In this model, the 3T cluster of the active site is embedded into the 84T crystal lattice of faujasite zeolite and, hence, it inherits the steric constraints of the nanostructured zeolite pores. As a result, the alkoxide intermediate in this model appears to be an active species that can readily become involved in the benzene alkylation.

A.2 Second step

After forming alkoxide intermediate, which is in stable complex in active site, it can react with benzene molecule via alkylation reaction to form ethylbenzene [eqs. (3)-(4)] (subsection A.2.1) or react with another ethylene molecule via dimerization to form butoxide [eq. (5)] (subsection A.2.2):

$$CH_3CH_2\text{–FAU} + C_6H_6 \rightleftharpoons (CH_3CH_2)C_6H_5\text{–H–FAU} \qquad \text{(eq.3)}$$

$$(CH_3CH_2)C_6H_5\text{–H–FAU} \rightleftharpoons (CH_3CH_2)C_6H_5 + \text{H-FAU} \qquad \text{(eq.4)}$$

$$CH_3CH_2\text{–FAU} + C_2H_4 \rightleftharpoons C_4H_9\text{–FAU} \qquad \text{(eq.5)}$$

A.2.1 Alkylation of alkoxide intermediate with benzene molecule

Step (3) involves the interaction of the alkoxide intermediate with benzene, resulting in adsorbed ethylbenzene which is desorbed in the step (4). Under typical reaction temperatures, ethylene readily adsorbs on the zeolite acid site and interacts strongly to the Brønsted acid site. On the other hand, the adsorbed

benzene weakly interacts with the acid site (although the benzene adsorption energy is high, most of it derives from van der Waals interactions with the zeolite pore walls) (Du *et al.,* 2002, Siffert *et al.,* 2000). In addition, with the adsorption experiments reported in the literature (Flego *et al.,* 1995, Venuto *et al.,* 1968) it can be concluded that the adsorption constant for benzene is small; therefore, it is possible to assume, for simplicity, that the competitive adsorption of benzene can be considered unimportant.

The reaction profile involving the reaction between the alkoxide intermediate with benzene to produce ethylbenzene is shown in Figure 17a and selected structural parameters are tabulated in Table 3. A benzene molecule diffuses into the vicinity to react with the alkoxide. The alkylation of benzene involves concerted bond forming between the carbon atoms of ethylene and benzene and the breaking of a benzene proton giving the proton back to the zeolite-bridging oxygen.

The vibrational motion corresponding to the imaginary frequency at the transition is explicitly shown in Figure 17b, which clearly demonstrates that the C–C bond forming between the ethyl and benzene occurs via interactions of surface ethoxide and benzene. During the transformation, the C–O covalent bond of the surface ethoxide is breaking while the bond between the ethyl and benzene begins to form and a benzene proton is leaving toward the zeolite framework. The activation energy is evaluated to be 38.18 kcal/mol. The adsorbed ethylbenzene product is subsequently desorbed endothermically, requiring energy of 20.11 kcal/mol.

Table 3 The optimized geometric parameters of benzene–alkoxide adsorption complex, transition state (TS2), and product ethylbenzene adsorption of step (3) on FAU using ONIOM3 (distances are in angstroms and angles are in degrees).

Parameters	Benzene-alkoxide	TS2	product
Distances			
C1-C2	1.501	1.505	1.531
C2-C3	3.810	1.819	1.509
C3-C4	1.395		1.406
C3-H2	1.082	1.173	2.208
C4-H2	1.079		2.417
O1-H2	2.486	1.581	0.985
C2-O2	1.521	2.932	3.693
Al-O1	1.701	1.730	1.858
Al-O2	1.881	1.775	1.698
Si1-O1	1.598	1.591	1.665
Si2-O2	1.682	1.608	1.599
Angles			
∠Si1O1Al	118.4	121.2	122.9
∠Si2O2Al	133.1	136.7	132.1

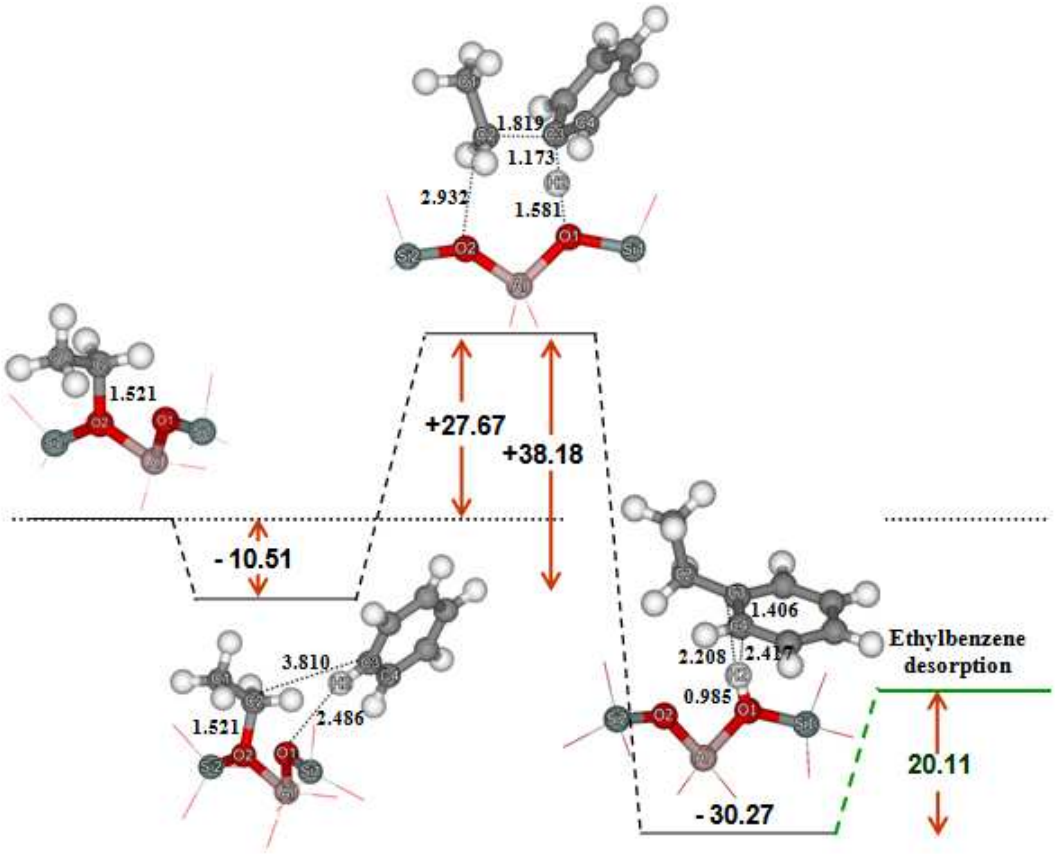

a)

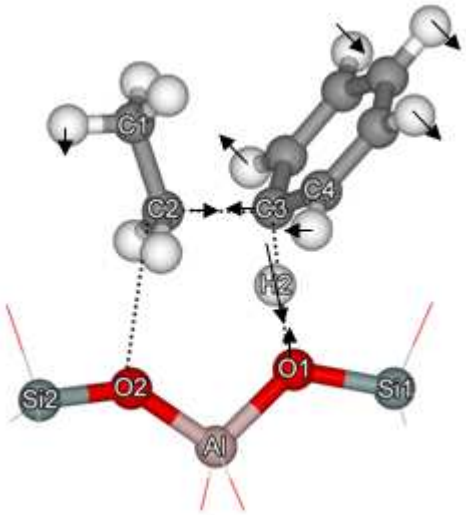

(b)

Figure 17 (a) Calculated energy profile for the second step of stepwise reactions for benzene alkylation. (b) Vibrational movement corresponding to the imaginary frequency at the transition structure.

A.2.2 Dimerization of alkoxide intermediate and ethylene molecule

Instead of reaction with the benzene molecule as in subsection A.2.1, ethoxide intermediate can react with another ethylene molecule to form a butoxide. The reaction profile is shown in Figure 18a, and the geometric parameters are listed in Table 4. The second ethylene molecule is adsorbed on the ethoxide intermediate and forms the ethylene–ethoxide complex. This complex is more stable than the ethoxide intermediate and has an adsorption energy of -12.83 kcal/mol. The co-adsorption of another ethylene molecule to some degree weakens the covalent ethoxide bonds, as seen from the lengthening of the C2–O2 bond from 1.521 to 1.530 Å. Then, the reaction proceeds by breaking of the covalent bond between the ethoxide species and the zeolite and formation of a new C–C bond to the second ethylene molecule.

The transition state for this reaction step has been identified, and the vibrational motion (Figure 18b) associated with the imaginary frequency shows that the reaction involves concerted bond breaking of O2–C2 and formation of the bond between C2 and C3. The transition-state structure shows that the covalent bond of the ethoxide with the zeolite oxygen atom is broken with a large increase of the C2–O2 bond length from 1.530 to 2.209 Å, and C2 is located about midway between the zeolite oxygen atom O2 and C3 of ethylene, where a new bond is forming. The C=C bond length of the second ethylene molecule is also significantly increased from 1.337 to 1.354 Å.

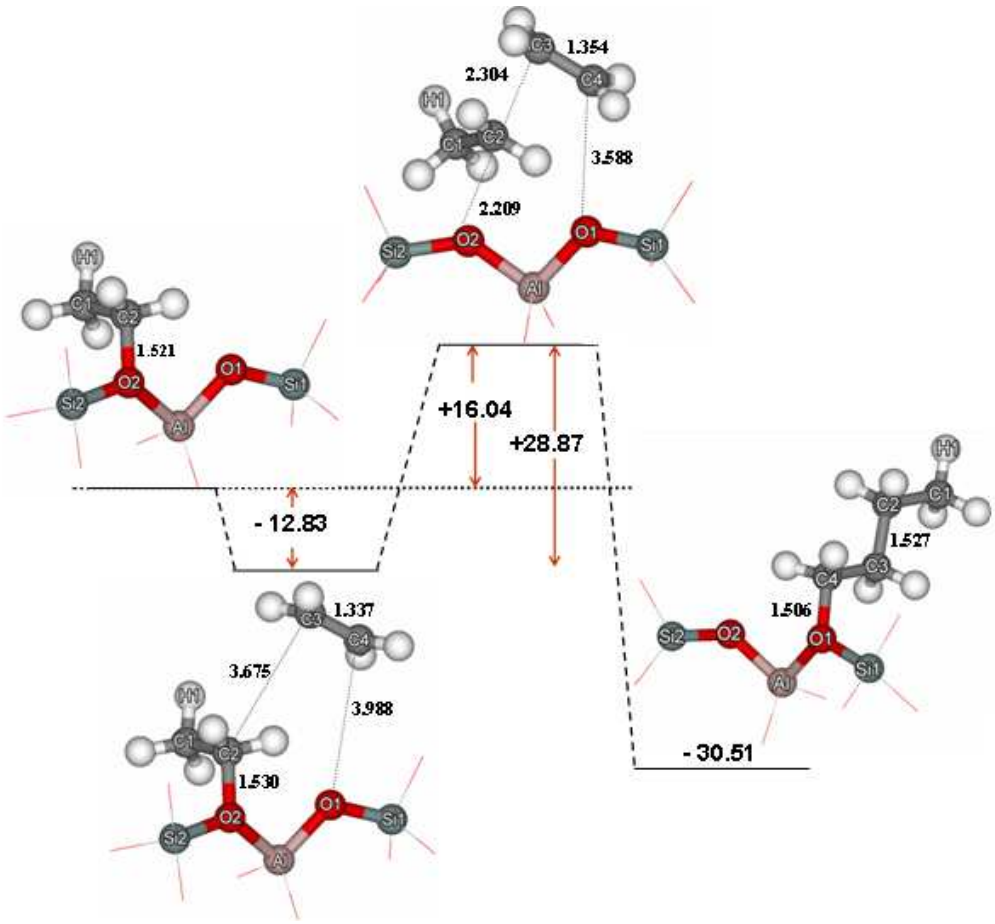

a)

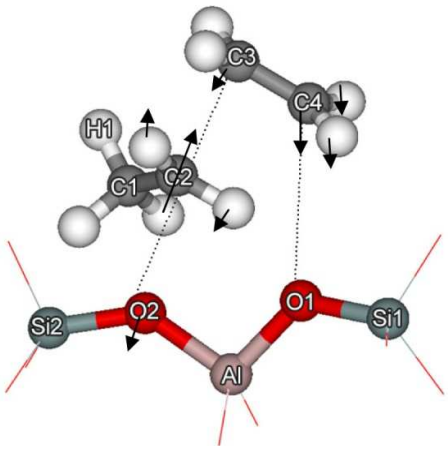

b)

Figure 18 (a) Calculated energy profile for the second step of stepwise for dimerization of alkoxide intermediate and ethylene molecule. (b) Vibrational movement corresponding to the imaginary frequency at the transition structure.

Table 4 The optimized geometric parameters of the ethylene-alkoxide adsorption complex, second transition state (TS2) and product butoxide of step 3 on faujasite (FAU) using the ONIOM3. Distances are in angstroms and angles are in degrees.

Parameters	Ethylene-alkoxide	TS2	Butoxide
Distances			
C1-C2	1.507	1.493	1.524
C2-C3	3.675	2.304	1.527
C3-C4	1.337	1.354	1.510
O1-C4	3.988	3.588	1.506
C2-O2	1.530	2.209	4.794
Al-O1	1.702	1.739	1.866
Al-O2	1.882	1.776	1.698
Si1-O1	1.595	1.595	1.670
Si2-O2	1.684	1.611	1.599
Angles			
∠Si1O1Al	118.7	121.2	120.5
∠Si2O2Al	132.3	135.8	133.4

The activation barrier for this step is calculated to be 28.87 kcal/mol, which is significantly lower than the values (44.74 kcal/mol) reported by Svelle (Svelle *et al.*, 2004). The discrepancy can be attributed to the difference in the relative stability and the weaker alkoxide bond found in this model as reflected by different alkoxide bond lengths (1.53 vs. 1.47 Å). Svelle used a small quantum cluster which represented a generic acidic zeolite but did not include the effect of the constraints of the zeolite pore. As a result, the ethoxide formed on the acid site was not subject to any steric interactions with the zeolite pore walls, so that it was bonded tightly to the acid site and became a stable intermediate. In contrast, in this ONIOM3 model, the ethoxide formed in the zeolite pore structure is destabilized by steric interactions with the zeolite walls and becomes a reactive species.

The butoxide produced by dimerization of ethylene is formed with a covalent bond to the zeolite framework. The overall reaction is highly exothermic by -39.48 kcal/mol. The butoxide product in this study is significantly less stable than that in the quantum cluster studies (-50.24 kcal/mol) (Svelle *et al.*, 2004). This is also possibly due to steric interactions of the butoxide with the zeolite walls.

B. Concerted mechanism

Alternatively, dimerization of ethylene and alkylation of benzene can proceed in a single step via the concerted interactions in the coadsorbed complex of ethylene with ethylene (in case of dimerization) and with benzene (in case of alkylation) without the formation of an alkoxide intermediate.

B.1 Concerted mechanism for alkylation of benzene with ethylene

The reaction steps can be written as follows:

$$C_2H_4 + H\text{–}FAU \rightleftharpoons C_2H_4\text{–}H\text{–}FAU \qquad \text{(eq.1)}$$

$$C_6H_6 + C_2H_4\text{–}H\text{–}FAU \rightleftharpoons (CH_3CH_2)C_6H_5\text{–}H\text{–}FAU \qquad \text{(eq.6)}$$

$$(CH_3CH_2)C_6H_5\text{–}H\text{–}FAU \rightleftharpoons (CH_3CH_2)C_6H_5 + H\text{-}FAU \qquad \text{(eq.7)}$$

Very recently, DFT cluster calculations of ethylbenzene formation via the concerted reaction of the co-adsorbed complex have been reported using DFT quantum cluster calculations by Vos *et al*. (Vos *et al.*, 2001) and Arstad *et al.* (Arstad *et al.*, 2004). Therefore, a comparison will be made and the effect of inclusion of the extended framework of the zeolite by the ONIOM method will be discussed.

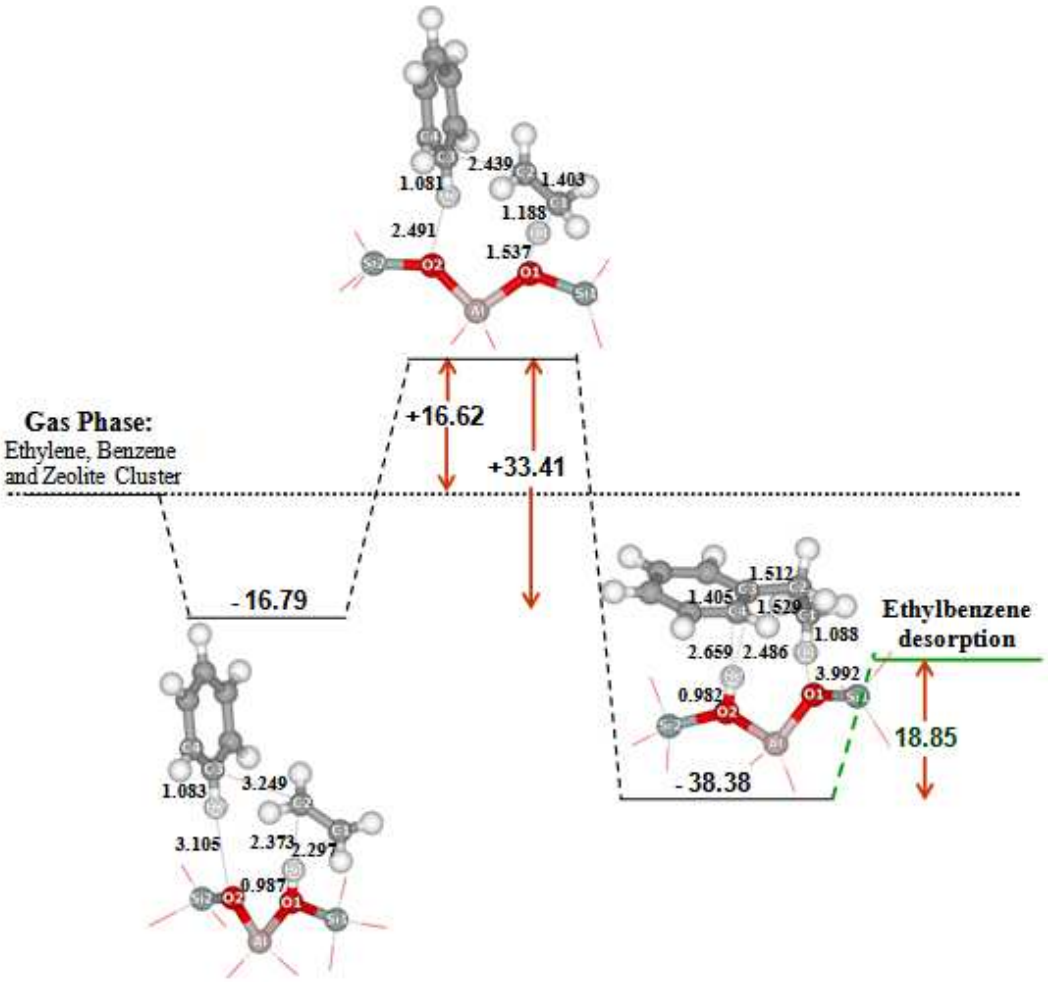

a)

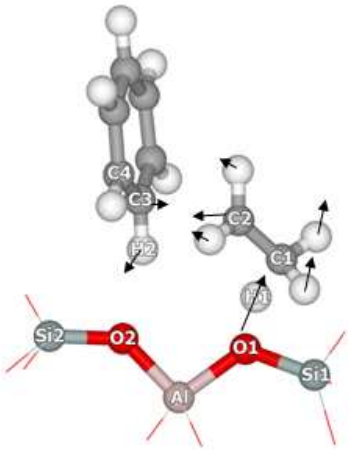

b)

Figure 19 (a) Calculated energy profile for the concerted of benzene dimerization. (b) Vibrational movement corresponding to the imaginary frequency at the transition structure.

The reaction energy profile is presented in Figure 19a and the selected geometrical parameters of intermediates and transition state are tabulated in Table 5. The reaction is initiated by co-adsorption of benzene on the adsorbed ethylene at the acid site of the zeolite. The co-adsorption energy is evaluated to be −16.79 kcal/mol, which is significantly higher than the values previously reported by Vos *et al*. and Arstad *et al*. (7.3 and 7.8 kcal/mol, respectively). The difference results mainly from van der Waals interactions between the adsorbed complex and the zeolite walls, which in this study were taken into account by using the UFF force field to model the extended framework of the zeolite (Bobuatong *et al.*, 2003, Clark *et al.*, 2003, Derouane *et al.*, 2000, Kasuriya *et al.*, 2003, Pelmenschikov *et al.*, 1999, Rozanska *et al.*, 2001, Vos *et al.*, 2001, Wesolowski *et al.*, 1997).

At the transition state, there is an imaginary frequency associated with the transition complex (Figure 19b) which indicates that the zeolitic proton (H1) is moving toward the ethylene carbon (C1) and the other ethylene carbon (C2) starts forming a bond with the benzene carbon (C3) and, simultaneously, the benzene proton is leaving toward the zeolite-bridging oxygen (O2). The vibrational motion of the transition state complex clearly indicates the concerted mechanism of the alkylation of benzene. The structure of the transition state shows that the Brønsted acid O1–H1 distance is greatly lengthened from 0.987 to 1.537 Å and the distance between the zeolitic proton (H1) and the ethylene carbon (C1) becomes 1.188 Å. The ethylene C–C bond distance is significantly lengthened from 1.342 to 1.403 Å, whereas the structure of the benzene molecule does not significantly differ from that of the co-adsorbed structure except that the distance between the benzene proton (H2) and the zeolite-bridging oxygen (O2) is shortened from 3.105 to 2.491 Å. The transition-state structure obtained in this model is similar to that of reported by Arstad *et al*. (2004), but slightly different from that reported by Vos *et al*. (2001) in which the ethylene is completely protonated at the transition state. The activation energy is calculated to be 33.41 kcal/mol, very close to the numbers reported by Vos *et al.* and Arstad *et al*. (31.6 and 31.3 kcal/mol, respectively).

Table 5 The optimized geometric parameters of isolated molecule, co-adsorption complex, transition state (TS), and product of concerted reaction of benzene alkylation on FAU using ONIOM3 (distances are in angstroms and angles are in degrees).

Parameters	Isolated cluster	Co-adsorption Complex	Transition State	Product
Distances				
Al-H1	2.462			
C1-C2	1.335	1.342	1.403	1.529
C2-C3	-	3.249	2.439	1.512
C3-C4	-	1.398	1.408	1.405
C3-H2	-	1.083	1.081	2.486
C4-H2	-	2.147	2.159	2.659
O2-H2	-	3.105	2.491	0.982
C1-H1	-	2.297	1.188	1.088
C2-H1		2.373	2.030	2.165
O1-H1	0.970	0.987	1.537	3.992
Al-O1	1.876	1.861	1.773	1.701
Al-O2	1.694	1.699	1.741	1.886
Si1-O1	1.669	1.667	1.612	1.601
Si2-O2	1.606	1.602	1.598	1.683
Angles				
∠Si1O1Al	123.7	122.9	121.7	116.9
∠Si2O2Al	130.4	131.5	134.9	135.1

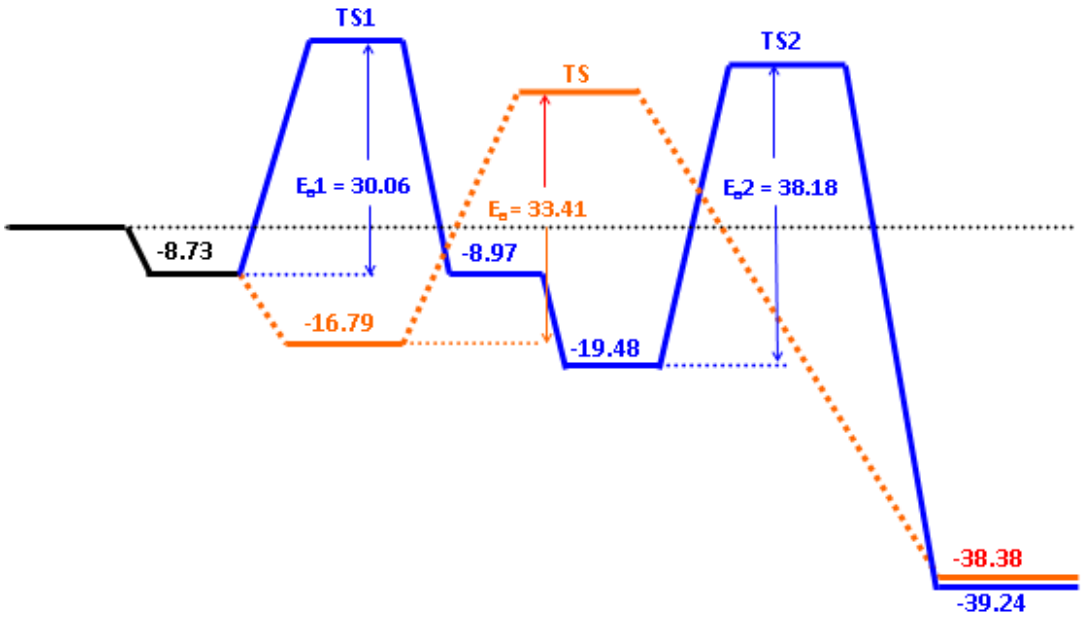

Figure 20 Calculated energetic profiles for the stepwise (solid line) and concerted (dashed line) reaction mechanisms of benzene alkylation with ethylene.

The complete energetic profiles of the two mechanisms are drawn on the same diagram (Figure 20) for easy comparison. For the stepwise mechanism, the alkoxide formation has a smaller activation energy of 30.06 kcal/mol and the surface reaction step is the rate-determining step with the activation energy of 38.18 kcal/mol. The activation barrier of the concerted mechanism of 33.41 kcal/mol is in between the barriers of the stepwise mechanism. It might appear that the concerted mechanism should dominate the overall alkylation reaction due to the smaller activation energy. However, the stepwise mechanism could also contribute significantly because, from an energetic point of view, the alkoxide formation will occur relatively easily, and after the alkoxide intermediate is formed the stability of the adsorbed benzene–alkoxide adduct makes the reverse reaction more difficult to occur than the forward reaction to the ethylbenzene product. When it is considered that both mechanisms can take place under the reaction conditions, the calculated apparent activation energy for the alkylation of benzene with ethylene would be in a range of 16.62–27.67 kcal/mol.

Although, there is no experimental value of the activation energy for alkylation of benzene with ethylene in zeolites to compare with, our computed

apparent activation energy range seems reasonable when compared with the apparent activation energies (10–18 kcal/mol) for alkylation of benzene with propylene in zeolites (Becker *et al.*, 1973, Corma *et al.*, 2000, Siffert *et al.*, 2000). Because ethylene is a poorer alkylating agent than propylene, and the rate of benzene alkylation with ethylene is much slower than that with propylene and generally it requires a higher reaction temperature to obtain the same conversion level as that of the alkylation with propylene (Corma *et al.*, 2000, Degnan Jr *et al.*, 2001, Du *et al.*, 2002, Vos *et al.*, 2003), the activation energy of the alkylation with ethylene is expected to be higher than the activation energy of the alkylation with propylene.

B.2 Concerted mechanism for dimerization of ethylene

Alternatively, protonation and C–C bond formation between the second ethylene molecule and the π-bonded adsorbed ethylene molecule occur simultaneously to give the butoxide product without formation of the ethoxide intermediate [Eqs. (1) and (8)]:

$$C_2H_4 + H\text{–}FAU \rightleftharpoons C_2H_4\text{–}H\text{–}FAU \qquad \text{(eq.1)}$$

$$C_2H_4 + C_2H_4\text{–}H\text{–}FAU \rightleftharpoons C_4H_9\text{–}FAU \qquad \text{(eq.8)}$$

The energy profile of the reaction is shown in Figure 21a, and selected geometrical parameters are listed in Table 6. The initial step starts with the adsorption of an ethylene molecule to give the weak π-adsorption complex. Then, another ethylene molecule is weakly co-adsorbed onto the π-complex by interaction of a carbon atom with the oxygen atoms of the zeolite. The C4–O1 and C4–O2 distances are calculated to be 3.724 and 3.849 Å, respectively. These weak interactions result in a small binding energy of -5.53 kcal/mol, which is lower than the binding energy of the p complex of -8.73 kcal/mol. The next step is the concerted protonation of the the π-adsorbed ethylene molecule by the zeolite proton and simultaneous formation of a C–C bond between the two ethylene molecules.

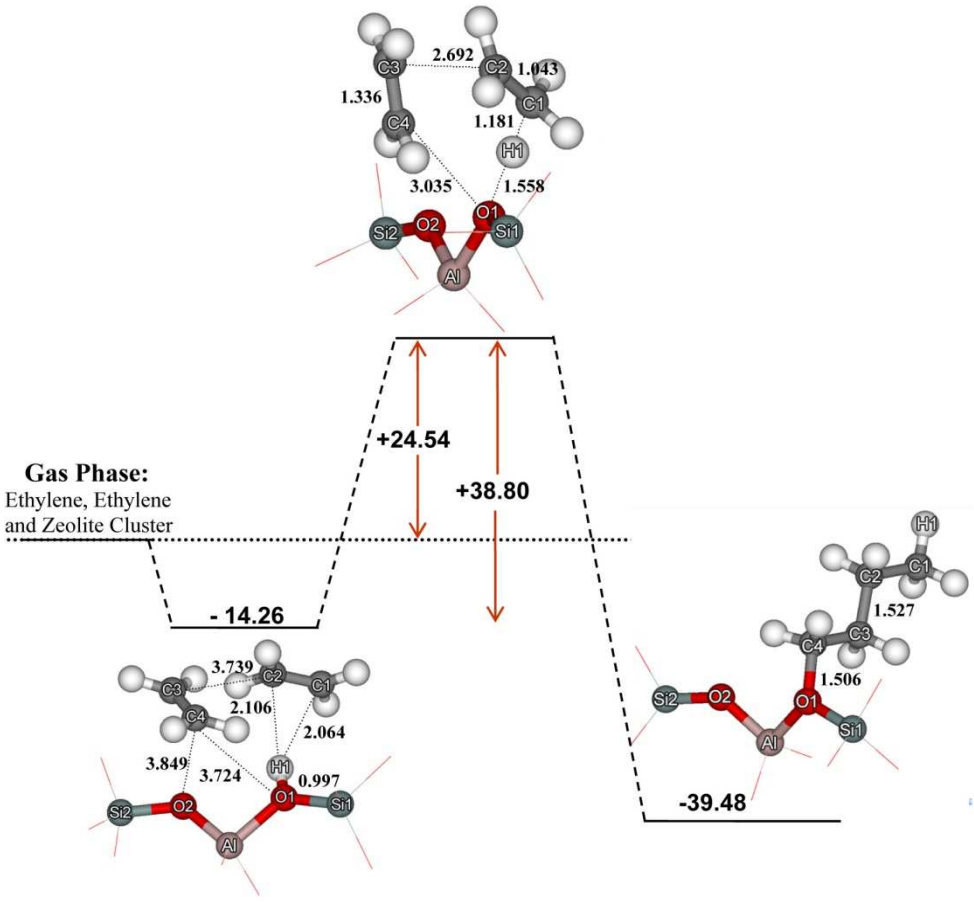

a)

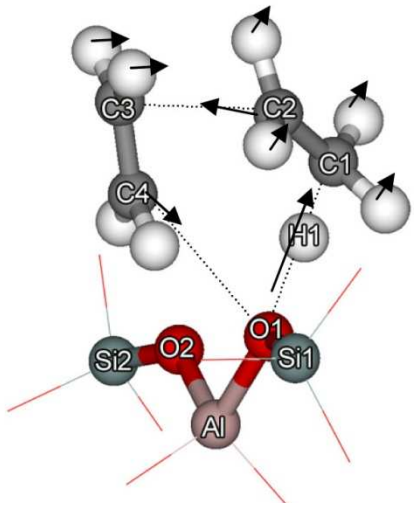

b)

Figure 21 a) Calculated energy profile for the concerted mechanism of ethylene dimerization. b) Vibrational movement corresponding to the imaginary frequency at the transition structure.

Table 6 The optimized geometric parameters of the isolated molecule, co- adsorption complex, transition state (TS) and product butoxide of concerted reaction of dimerization of ethylene on faujasite (FAU) using the ONIOM3. Distances are in angstroms and angles are in degrees.

Parameters	Co-adsorption Complex	Transition State	Butoxide
Distances			
C1-C2	1.344	1.403	1.524
C2-C3	3.739	2.692	1.527
C3-C4	1.336	1.346	1.510
C4-O1	3.724	3.035	1.506
C4-O2	3.849	3.256	2.929
C1-H1	2.064	1.181	1.088
C2-H1	2.106	2.075	2.170
O1-H1	0.997	1.558	5.919
Al-O1	1.858	1.769	1.866
Al-O2	1.701	1.743	1.698
Si1-O1	1.659	1.612	1.670
Si2-O2	1.602	1.597	1.599
Angles			
∠Si1O1Al	123.4	121.6	120.5
∠Si2O2Al	131.4	135.5	133.4

At the transition state, the acidic proton of the zeolite has partially protonated the carbon atom of the ethylene molecule, as indicated by the shorter distance of H1 to the ethylene carbon atom than to O1 of the zeolite (1.181 vs. 1.558 Å), while the C–C bond between the ethylene molecules is forming. The C1=C2 and C3=C4 bond lengths are increasing and the new bonds between C2 and C3 and C4 and O1 are forming, leading to the formation of the butoxide. The frequency analysis (Figure 21b) shows vibrational movement of atoms at the transition state which corresponds well with the concerted mechanism as described above, and also shows

that the C4 atom is moving toward O1 of the zeolite, that is, the butoxide product forms a covalent bond to O1 where the acidic proton was previously located. The partially protonated transition-state structure was also reported by Svelle *et al*. (Svelle *et al.*, 2004) for concerted dimerization of ethylene, but in their report the distance between the second ethylene molecule and the zeolite acid site appears to be farther than in our study. The activation energy is evaluated to be 38.80 kcal/mol, which agrees well with the value of 39.3 kcal/mol reported by Svelle *et al.* at comparable level of theory [MP2/6-311G(d,p)//B3LYP/6-31G(d)]. It has been pointed out that for acid-catalyzed reactions, the activation energy of the reaction step involving protonation depends on the degree of proton transfer at the transition state (Svelle *et al*., 2003, Rozanska *et al*., 2002, 2003, Boronat *et al*., 2001, 2004). Generally, longer O1−H1 and shorter H1−C1 distances indicate more advanced proton transfer and higher activation energy. In this mechanism, the transition state has a significant degree of proton transfer, and thus the activation energy is mainly due to removal of the acidic proton from the zeolite. Therefore, it is not unexpected that the activation energies obtained from the quantum cluster and ONIOM calculations are comparable.

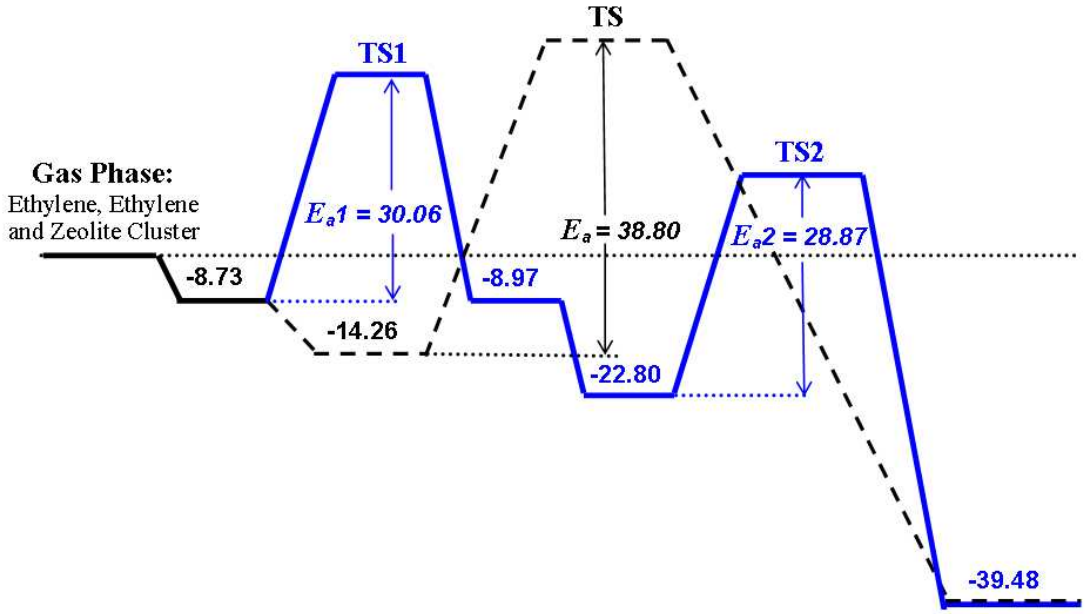

Figure 22 Calculated energy profiles for the stepwise (solid line) and concerted (dashed line) reaction mechanisms of ethylene dimerization.

For convenient comparison, the complete energetic profiles of both possible mechanisms are shown on the same diagram (Figure 22). In the stepwise mechanism, the protonation of the adsorbed ethylene is a rate-determining step with an activation barrier of 30.06 kcal/mol. The resulting ethoxide is destabilized by van der Waals interactions with the zeolite walls and thus active for further reactions. The subsequent reaction of the ethoxide with another ethylene molecule is more facile than the protonation step, and the activation barrier for this step is 28.87 kcal/mol. For the concerted mechanism, the activation barrier is calculated to be 38.80 kcal/mol, which is significantly higher than the energy barrier of the rate-determining step of the stepwise mechanism. Moreover, the relative energy of the transition state of the concerted mechanism is higher than both transition states in the stepwise mechanism.

The zeolite environment included by the ONIOM method affects the stability of the adsorbed species inside the zeolite and, most importantly, significantly alters the stability of the surface alkoxide species, which appears to be a key intermediate for this reaction. Therefore, from the energetics of the reactions and relative stability of transition states, it can be concluded that the stepwise mechanism should dominate the overall reaction of the dimerization of ethylene, which is in agreement withth e experimental results (Geobaldo *et al.*, 1997, Spoto *et al.*, 1994) that dimerization of ethylene and propylene over H-mordenite and H-ZSM-5 proceeds in stepwise manner via alkoxide intermediates.

3. Structures and reaction mechanisms of propene oxide isomerization

3.1 The zeolite models and adsorption complexes

The 5T and 46T clusters are shown in Figure 11 while their geometric parameters are tabulated in Table 7. To observe the catalytic framework effect on the reaction over the active site, the atoms in the 5T region in both clusters have been optimized with the exception of the atoms in the extended framework of the ONIOM model, which were fixed. Comparison of the 5T quantum cluster and the 46T ONIOM model reveals little difference in the geometric parameters. As the extended framework has only a small effect on the active site geometry by decreasing the Brønsted acid angle (Al-O1-Si1) by about 1° and slightly lengthening the O1-H1 bond distance, the indication is that the active site in the 46T ONIOM model might be more acidic than that in the 5T quantum cluster, which, inturn, leads to the prediction that the adsorption energy of adsorbates on the ONIOM model should also be higher.

The adsorption complexes of the propene oxide, propanal and propanone, which are the reactant and products for the isomerization of propene oxide, on the Brønsted acid site of the ZSM-5 zeolite in the quantum cluster and ONIOM model are depicted in Figure 23. These adsorbates interact on the acidic proton of zeolite via hydrogen bonding, and the geometric structures of all adsorption complexes are slightly deviated from those of isolated structures (Table 8).

Table 7 The optimized geometric parameters of the zeolite 5T and 46T clusters calculated at B3LYP/ 6-31G(d,p) and ONIOM(B3LYP/6-31G(d,p):UFF) levels.[a]

Parameters	5T	46T
	Distances	
O1-H1	0.969	0.970
Al-O1	1.853	1.786
Al-O2	1.703	1.656
Al-O3	1.687	1.637
Al-O4	1.687	1.649
Si1-O1	1.694	1.670
Si2-O2	1.620	1.592
Si1-O3	1.627	1.597
Si2-O4	1.615	1.574
	Angles	
∠Si1O1Al	131.6	132.4
∠Si2O2Al	130.0	131.5
∠Si3O3Al	135.3	134.9
∠Si4O4Al	151.8	143.8

[a] Distances are in angstroms and angles are in degrees.

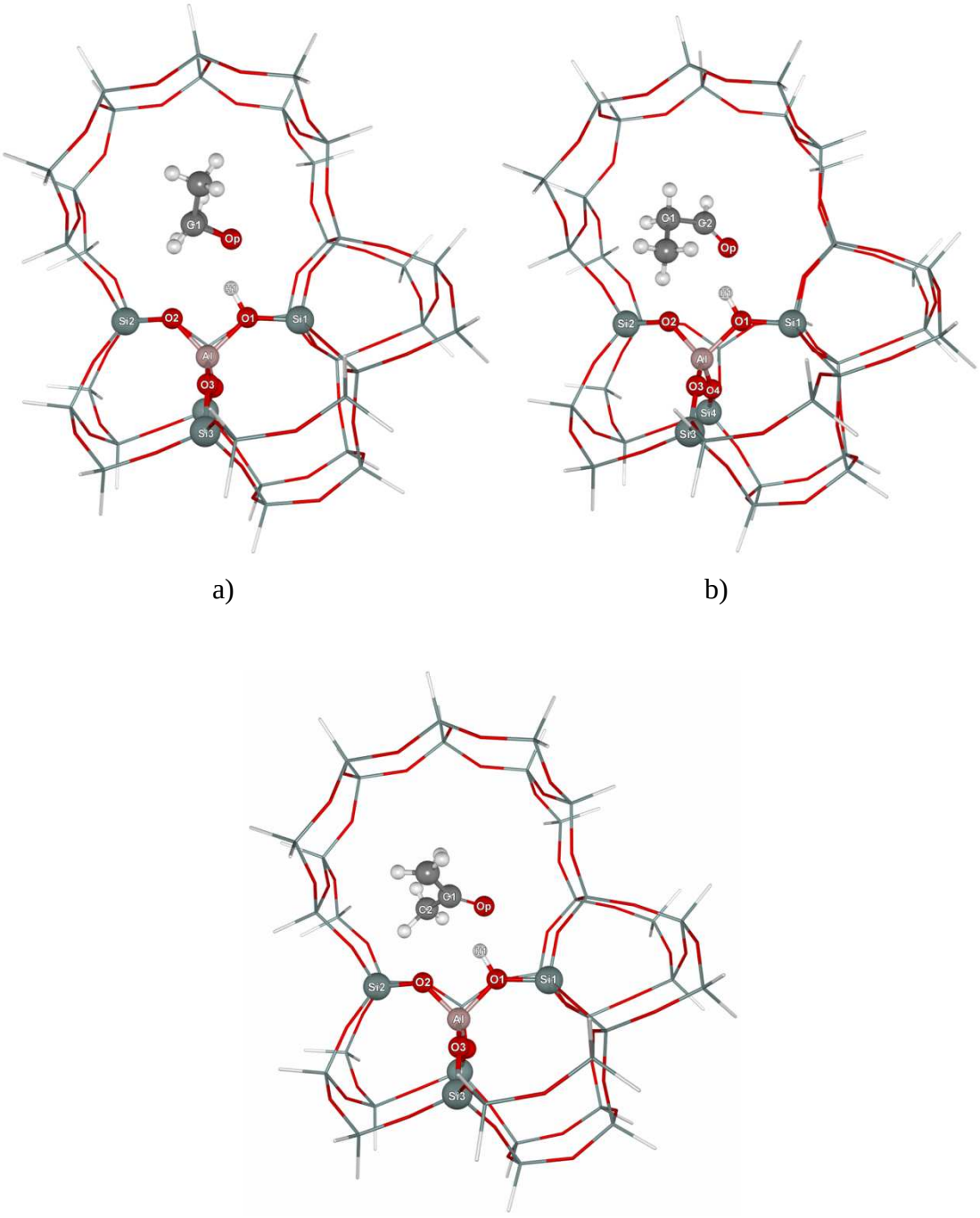

a) b)

c)

Figure 23 Presentation of models of ZSM-5 and its interaction with adsorbates: ONIOM2 layer models of 46T cluster interacts with (a) propene oxide, (b) propanal, and (c) propanone.

Table 8 The relevant parameters for the propene oxide, propanal, and propanone Adsorbed on 5T and 46T H-ZSM-5 zeolite clusters.

	distances (Å)					
	O1-Hz	Op-Hz	C2-Op	C1-C2	C1-Op	ΔE_a
isolated propene oxide			1.434	1.47	1.435	
Propene oxide on 5T	1.023	1.533	1.452	1.468	1.464	-16.8
Propene oxide on 46T	1.023	1.54	1.449	1.468	1.461	-30.8
isolated	1.211	1.512	2.419			
Propanal on 5T	1.004	1.614	1.222	1.498	2.435	-15
Propanal on 46T	1.015	1.585	1.225	1.493	2.416	-26.3
isolated	2.394	1.52	1.216			
Propanone on 5T	1.025	1.527	2.393	1.506	1.232	-16.7
Propanone on 46T	1.039	1.476	2.4	1.506	1.233	-30.4[a]

[a] The propanone (acetone) adsorption on H-ZSM-5 from experimental data is -31.1 kcal/mol (Sepa *et al*., 1996). ΔE_a stands for adsorption energy (kcal/mol).

In the propene oxide adsorption complex (Figure 23a), the oxygen atom of propene oxide interacts with the acidic proton via hydrogen bonding with the Op-H1 distance of 1.540 Å (cf. Table 8). The hydrogen bonding interaction lengthens the Brønsted acid O1-H1 bond distance by 0.054 Å. Although the epoxide ring is asymmetric, the epoxide ring center aligns above the acidic site with almost equal distances of C1-O1 and C2-O1 and C1-O2 and C2-O2. Because of the decrease of the electron density on Op via the electron transfer from the Op to the H1 atom, the C1-Op and C2-Op bonds are elongated by 0.026 and 0.015 Å, respectively. The greater increase in the length of the C1-Op bond leads to the prediction that it would be broken more easily than the shorter C2-Op bond. The adsorption energy is evaluated to be -16.8 and -30.8 kcal/mol for the 5T quantum cluster and ONIOM calculations, respectively. The propanal and propanone also adsorb on the acidic proton of zeolite via hydrogen bonding (see Figure 23b and 23c). Since the carbonyl CdOp bonds are strong double bonds, they are not changed significantly during the adsorption on the

active site of zeolite. The CdOp bond of the propanone adsorption complex alters slightly from isolated propanone by 0.017 Å, and that of the propanal is changed by only 0.008 Å (cf. Table 7). The hydrogen bonding interaction lengthens the Brønsted acid O1-H1 bond distance by 0.046 and 0.068 Å for the adsorption of propanal and propanone, respectively. The adsorption energies of propanal and propanone are evaluated to be -15.0 and -16.7 kcal/mol for the quantum cluster and -26.3 and -30.4 kcal/mol for the ONIOM model, respectively. The framework effect in the ONIOM model approximately doubles the adsorption energies of the adsorption complexes. The van der Waals interactions between the adsorbates and the zeolite pore walls stabilize the adsorption complexes inside.

The calculated adsorption energy of propanone of -30.4 kcal/mol compares well with the experimental data of -31.1 kcal/mol (Sepa *et al.*, 1996). This result indicates that the combination between the B3LYP density functional theory at the active region and UFF force field at the extended framework in the ONIOM model can produce reasonable interaction energies between these adsorbates and the zeolite catalyst (Namuangruk *et al*., 2006a, 2006b). Therefore, this ONIOM model should be suitable to use for investigation of the isomerization reaction for this system.

3.2 The reaction mechanism of isomerization of propene oxide

The isomerization mechanism of propene oxide to carbonyl compounds is considered to occur via the C-O bond breaking of the oxirane ring in the propene oxide molecule. The asymmetric structure of propene oxide has two different C-O bonds (more or less substituted carbon atom sides) that can be broken and, thus, has two possible products of the ring opening reaction: propanal and propanone. Propanal is formed via the C-O bond breaking at the tertiary carbon atom (C1-Op), while propanone is formed via the C-O bond breaking at the other carbon atom (C2-Op) in the oxirane ring (cf. Figure 23). To elucidate the explanation and represent it in a more instructive format, the detailed mechanism will be separated into two subsections.

A. The reaction mechanism leading to propanal

The isomerization mechanism of propene oxide to propanal on H-ZSM-5 zeolite has been proposed as a stepwise reaction processes. The calculated energy profile for the isomerization of propene oxide to propanal is shown in Figure 24a and the calculated relative energies and activation energies are shown in Table 9. First, the propene oxide molecule diffuses into the pore of zeolite and then adsorbs on the acidic proton at the active site to form the propene oxide adsorption complex. Propene oxide adsorbs on the acidic proton via hydrogen bonding with the Op-H1 distance of 1.540 Å and the adsorption energy of -30.8 kcal/mol. In this adsorption complex, the C1-Op and C2-Op bond lengths are calculated to be 1.461 Å and 1.449 Å, respectively. Then, the C1-Op bond is broken to produce the secondary alkoxide intermediate (Int_A) through the secondary carbenium ion transition state (TS1_A).

At the TS1_A transition-state configuration, the acidic proton of the zeolite is protonated to the adsorbed propene oxide, the C1-Op bond is broken, and the hybridization of C1 is changed from tetrahedral (sp^3) to planar (sp^2). The transition state (cf. Figure 24b) can be confirmed by the frequency calculation with one imaginary frequency at -224.8 cm^{-1}, which is related to the movement of the acidic proton of zeolite (H1) to the propene oxide oxygen (Op) and the breaking of C1-Op bond. The calculated energy barrier for this ring-opening step is 38.5 kcal/mol and the apparent activation energy is 7.7 kcal/mol. The secondary alkoxide intermediate (Int_A) is attached to the oxygen atom (O2) of the zeolite and is stabilized by the zeolite framework.

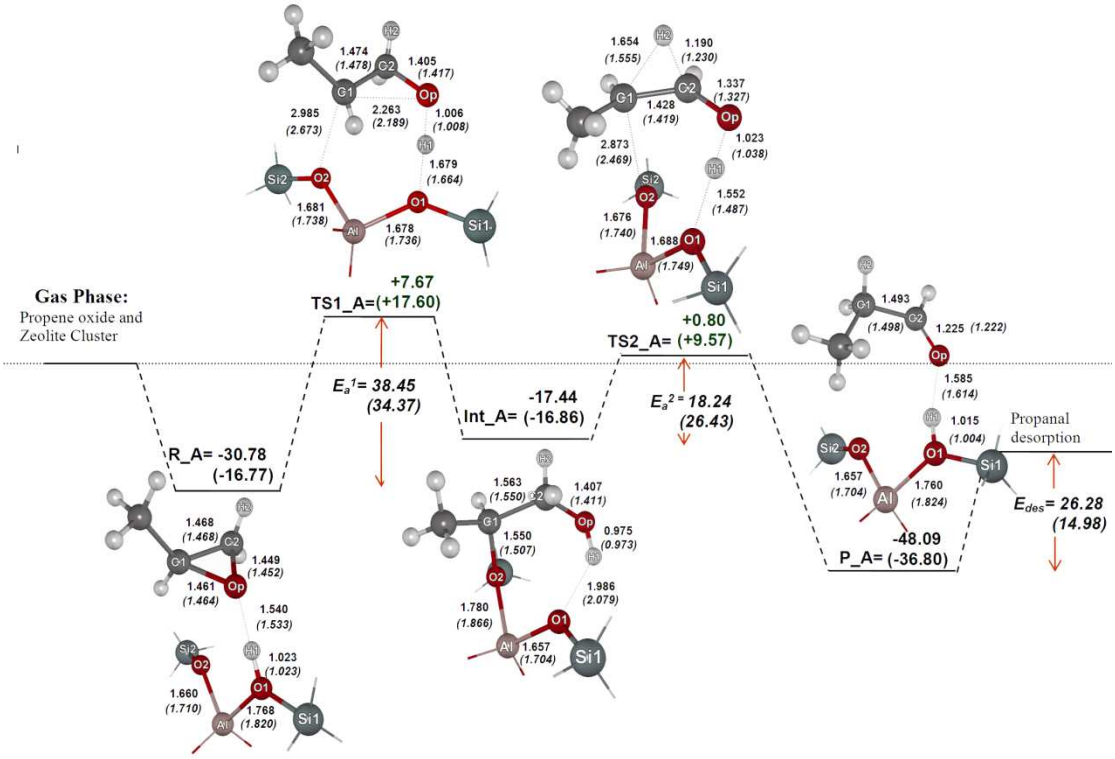

a)

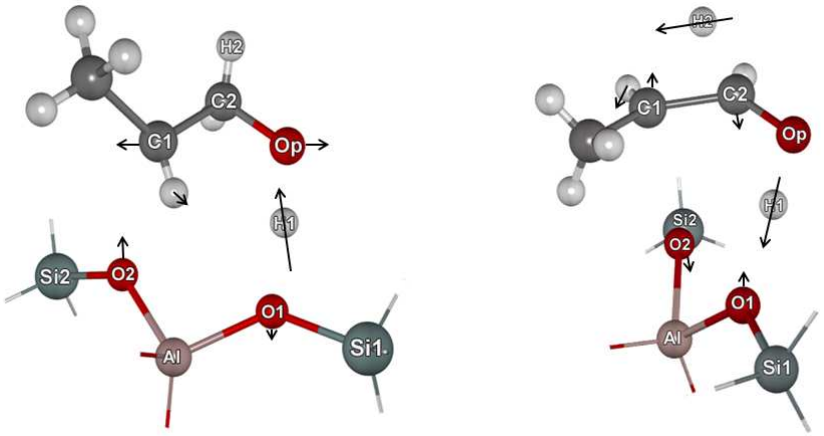

b) c)

Figure 24 a) The calculated energy profile for the isomerization of propene oxide to propanal over 46T and 5T (in parentheses) clusters; b) the vibrational movement corresponding to the imaginary frequency at the TS1_A; c) the vibrational movement corresponding to the imaginary frequency at the TS2_A.

The next step is the carbonyl-forming step, which involves the transformation of the Int_A intermediate to the adsorbed propanal (P_A) via the 1,2-hydride shift. At this transition-state configuration (TS2_A), the H2 atom is moving toward the carbon atom C2 placed with the C2-H2 and C1-H2 distances being 1.190 Å and 1.654 Å, respectively. The H1 atom is located in-between the O1 and Op atoms with Op-H1) 1.023 Å and H1-O1) 1.552 Å. Figure 24c depicts the vibrational motion that occurs at the TS2_A transition state which possesses one imaginary frequency at -770.6 cm^{-1}. This movement corresponds to the H2 atom transfer from C1 to C2 simultaneously with the C1-O2 covalent bond breaking and the H1 transfer from Op back to O1 to restore the active site of the zeolite. The activation energy for this step is calculated to be 18.2 kcal/mol and the propanal product is adsorbed on the acidic site of the ZSM-5 zeolite with the adsorption energy of -48.1 kcal/mol. Finally, the adsorbed propanal is desorbed endothermically and requires an energy of 26.3 kcal/mol.

Previously, Coxon and co-worker (1997) studied the isomerization of protonated propene oxide to protonated propanal and reported that the reaction followed the concerted asynchronous mechanism. The authors observed that the hydride migration did not occur until the ring-opening step was completed, although the authors did not find the carbenium ion intermediate. However, for the isomerization of protonated methyl propene oxide, the authors were able to find the more stable tertiary carbenium ion intermediate and reported that the reaction was stepwise (Coxon *et al.,* 1999). In this study, the reaction takes place inside the zeolite pore environment. Although the zeolite does not directly protonate the propene oxide, the hydrogen bonding interaction with the zeolite helps to facilitate the ring-opening reaction. Moreover, the adjacent O2 atom of the zeolite can help to stabilize the ring-opening intermediate carbenium ion by forming the stable alkoxide intermediate as it has been observed that surface alkoxide species are important reaction intermediates in many reactions in zeolites (Geobaldo *et al.,* 1997, Lesthaeghe *et al.,* 2005, Nieminen *et al.,* 2005).

Table 9 The calculated relative energies (kcal/mol) of reactant, first-transition state (TS1), intermediate, second-transition state (TS2), product, first activation energy barrier (ΔEa_1), and second activation energy barrier (ΔEa_2) for the isomerization reaction of propene oxide over 5T and 46T clusters of H-ZSM-5 calculated at B3LYP/6-31G(d,p) and ONIOM (B3LYP/6-31G(d,p): UFF) levels.

	5T cluster		46T cluster	
	propanal	propanone	propanal	propanone
Reactant	-16.8	-16.8	-30.8	-30.8
TS1	17.6	24.5	7.7	11.6
Intermediate	-16.9	-21.6	-17.4	-24.5
TS2	9.6	7.8	0.8	-1.3
Product	-36.8	-46.3	-48.1	-60.0
Product	-15.0	-16.7	-26.3	-30.4
ΔEa1	34.4	41.3	38.5	42.4
ΔEa2	26.5	29.4	18.2	23.2

Although all geometric parameters calculated from the quantum cluster (written in parentheses in Figure 24a) are quite similar to those obtained from the ONIOM model, the calculated relative energies and energy barriers differ considerably from the ONIOM results. It may seem surprising that the ONIOM and the cluster calculations give almost the same relative energy for the alkoxide intermediate (Int_A). This is derived by the erroneous prediction of relative stability of the alkoxide species by the cluster calculation. Since the structure of the small cluster can be significantly changed to accommodate the formation of the alkoxide, the alkoxide species can form a stronger covalent bond to the zeolite cluster. The covalent C-O bond distance in the cluster calculation is 1.507 Å which is shorter than the C-O bond of 1.550 Å in the case of the ONIOM model, and the zeolite O2AlO1 angle is 95.8 degrees in the cluster model while the O2AlO1 angle is 96.5 degrees in the ONIOM calculations. As a result, the covalent bond stabilization of the alkoxide in the small cluster is overestimated. The influence of the local geometry of zeolite on

the stability of alkoxide intermediates has been extensively discussed by Boronat *et al.* (Boronat *et al.*, 2001) Thus, it is indicated that a small quantum cluster can predict only the geometrical characters of the stationary points along the reaction pathway. However, for the energetic profile of the reaction, the ONIOM approach that takes into account the zeolite framework effects should be more suitable. The cause of these differences between the two models is the van der Waals effect from the zeolite framework acting on the adsorbate species at each stationary point.

B. The reaction mechanism leading to propanone

The isomerization of propene oxide can also produce propanone by breaking the less substituted C-O bond at the ring-opening step. The calculated energy profile for this route is illustrated in Figure 25a. The reaction starts with the adsorbed propene oxide (R_B) on the acidic proton of the zeolite. Subsequently, an adsorbed propene oxide is protonated at the Op atom and the less substituted C2-Op bond is broken leading to the formation of the primary alkoxide intermediate through the transition-state TS1_B, which possesses a primary carbenium ion configuration, which is less stable than the secondary carbenium ion (TS1_A) in the propanal route. This justification has been supported by the higher calculated energy barrier and apparent energy for the primary carbenium ion (TS1_B) which is evaluated to be 42.4 and 11.6 kcal/mol, respectively. The transition-state TS1_B has been verified by one imaginary frequency at -389.7 cm^{-1}, which involves the following movement (Figure 25b): the acidic proton transfers from the zeolite framework to the oxygen atom of propene oxide and the C2-Op bond breaks simultaneously as the covalent bond between C2 and O2 forms. At the transition-state configuration, it is observed that a H1 atom moves from O1 close to Op with the Op-H1 distance of 1.007 Å and the O1-H1 distance of 1.637 Å.

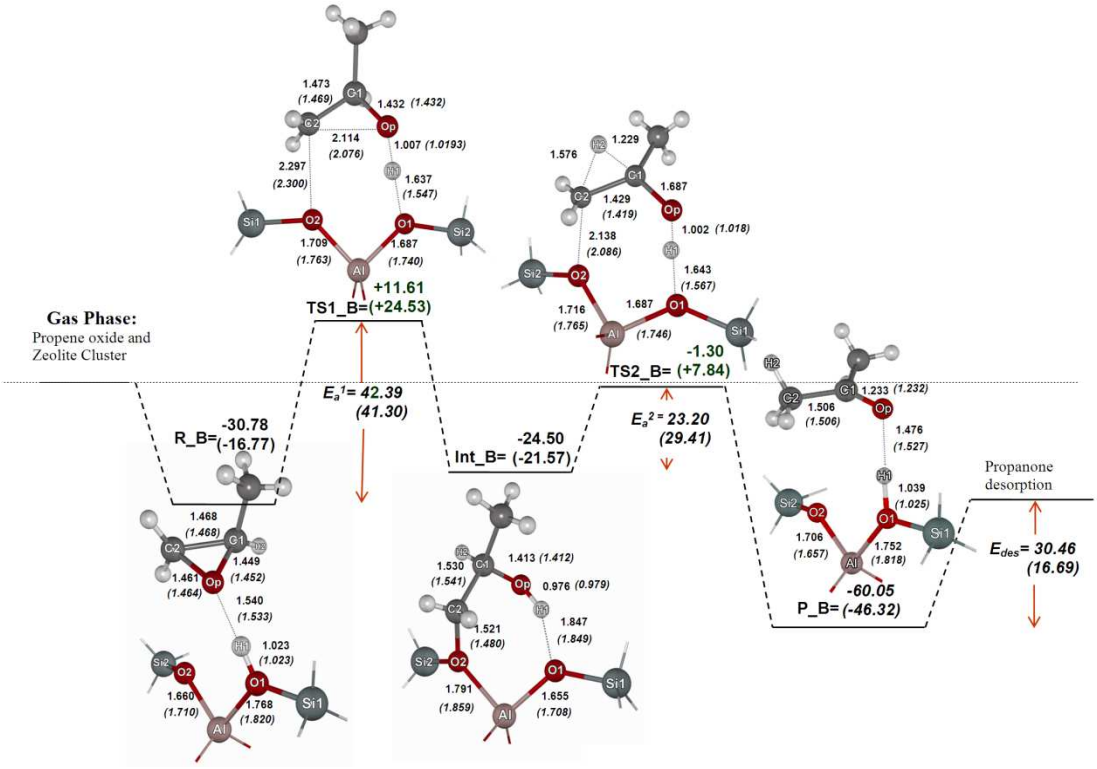

a)

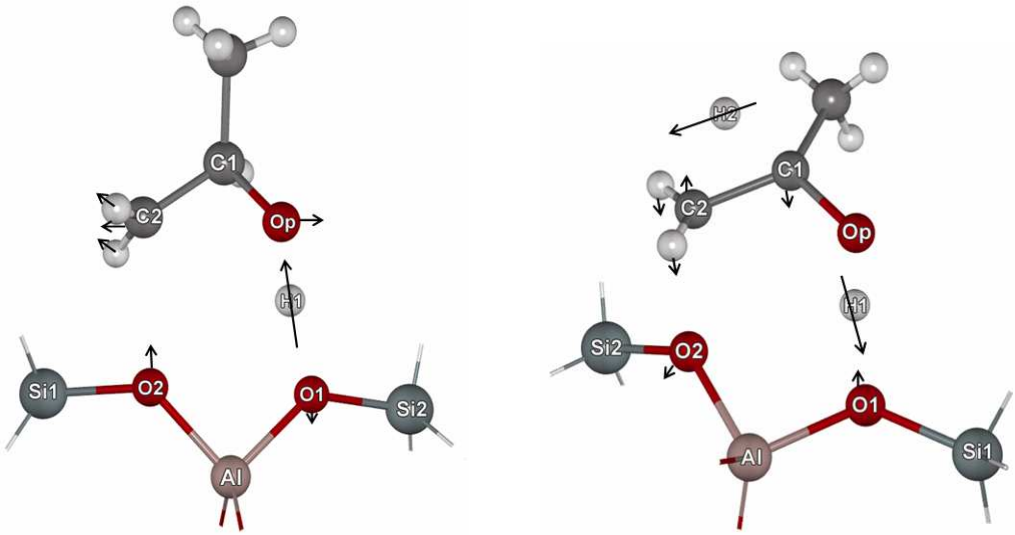

a) b)

Figure 25 a) The calculated energy profile for the isomerization of propene oxide to propanone over 46T and 5T (in parentheses) clusters; b) the vibrational movement corresponding to the imaginary frequency at the TS1_B; c) the vibrational movement corresponding to the imaginary frequency at the TS2_B.

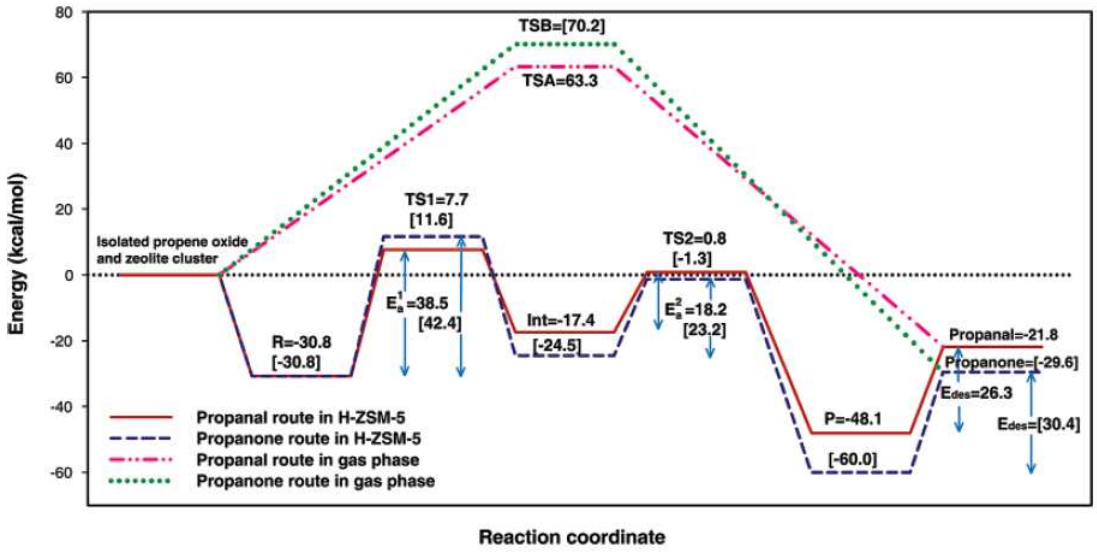

Figure 26 The energy profile of the isomerization of propene oxide to propanal on H-ZSM-5 zeolite (solid line), to propanone on H-ZSM-5 zeolite (dash line) calculated at ONIOM(B3LYP/6-31G(d,p):UFF), to propanal in gas phase (dash dot dot line), and to propanone in gas phase (dot line) calculated at B3LYP/6-31G(d,p).

The binding energy of the primary alkoxide intermediate (Int_B) is calculated to be 24.5 kcal/mol, which is more stable than that of the secondary alkoxide intermediate (Int_A) by 7.1 kcal/mol, resulting from the less steric disturbance effect from the substituted group on the alkoxide carbon atom. This less steric hindrance on the alkoxide carbon atom allows the adsorbate to move closer to the active site of the zeolite in comparison to the more steric one, C2-O2) 1.521 Å for the primary alkoxide (Int_B) and C1-O2) 1.550 Å for the secondary alkoxide (Int_A), respectively. Therefore, in the zeolite framework, the less steric alkoxide (Int_B) is more stable than the more steric alkoxide (Int_A). This observation is also in agreement with previous reports that the stability of the alkoxide intermediate formed in the zeolite structure is very sensitive to the local geometry of the active site and the nature of the alkoxide carbon atom (Boronat *et al.*, 1998, Boronat *et al.*, 2004, Boronat *et al.*, 2001). When the degree of substitution on alkoxide carbon increases, the covalent C-O bond distance is lengthened and the alkoxide is destabilized. The primary alkoxide intermediate (Int_B) is transformed to the adsorbed propanone

product (P_B) via the 1,2-hydride shift process through the transition state (TS2_B) which indicates that the distance of the breaking of the C1-H2 bond is 1.229 Å, the forming of the C2-H2 bond is 1.576 Å, while the breaking C2-O2 covalent bond is lengthened from 1.521 to 2.138 Å. Consequently, H1 moves back to the bridging oxygen atom by locating midway between Op and O1. The O1-H1 bond is shorter than Op-H1 bond, 1.039 and 1.476 Å, respectively. This vibrational movement, which corresponds to the imaginary frequency at -861.5 cm^{-1}, is depicted in Figure 25c. The energy barrier is calculated to be 23.2 kcal/mol, which is higher than that of the propanal route by 5.0 kcal/mol. Finally, the adsorbed propanone is desorbed endothermically, requiring a desorption energy of 30.4 kcal/mol.

For ease of comparison, the complete energetic profiles for all mechanisms are shown in the same diagram (Figure 26). This diagram shows the energies obtained from the ONIOM model, which include the zeolite framework effect and the gas-phase noncatalyzed isomerizations for comparison. Without a catalyst, the gas-phase propene oxide isomerization occurs via a single concerted step with high reaction barriers of 63.3 and 70.2 kcal/mol for the formation of propanal and propanone, respectively. It is undoubtedly observed that H-ZSM-5 zeolite alters the propene oxide isomerization mechanism to go through a series of steps with lower reaction barriers. The reaction starts with propene oxide adsorbed on the acid proton of zeolite. The ring opening step is considered to be the rate-determining step. The activation energies are 38.5 and 42.4 kcal/mol for propanal and propanone formation, respectively. The reaction intermediates and transition states are greatly stabilized by the zeolite framework. The transition states of this rate-determining step only lie above the reactants by 7.7 and 11.6 kcal/mol for propanal and propanone formation, respectively. The step following is the energy barrier for carbonyl forming, which involves the 1,2-hydride shift on connecting the C-C bond, and is evaluated to be 18.2 and 23.2 kcal/mol for propanal and propanone, respectively. Therefore, it can be concluded, by considering the relative reaction barrier and the transition-state stability, that the propanal is more favorably formed than the propanone. However, since the confinement effect of the H-ZSM-5 zeolite stabilizes the transition states and intermediates for both routes, the preference against the rupture of the more sterically

hindered C-O bond is not very high. This finding corresponds well with the experimental results10 that propanal was produced in a higher yield than that of propanone but the minor product, propanone, was also produced in a significant yield for the propene oxide isomerization in H-ZSM-5 zeolites.

4. Decomposition of nitrous oxide

In this topic (Namuangruk *et al*., 2007), the B3LYP/6-31G(d) was performed to investigate the reaction mechanisms of the decomposition of the nitrous oxide molecule on the perfect (Section 3.1) and the Stone–Wales defective (Section 3.2) models. The effect of a chloride anion encapsulated in the SWNTs on the reactivity of both perfect and defective tubes is also discussed in Section 3.3.

4.1 Reaction mechanisms on the perfect (5,5) SWNT

For an asymmetric N_2O molecule, the N–O and N–N bond lengths are measured to be 1.192 and 1.135 Å, respectively, which are in good agreement with the experimental data of 1.184 and 1.128 Å, respectively. By comparison, the relevant theoretical to experimental studies (Lu *et al.*, 2002b, Su *et al.,* 1999), show evidence to prove that five-membered heterocycles can be formed in the cycloaddition of 1,3-dipole N2O with double bonds in ethylene and surface diamond, implying that the double bond of carbon nanotubes could also form the five-membered ring with N_2O. In this work, the decomposition of nitrous oxide is investigated on the sidewall of SWNT by delivering the O atom in a N_2O molecule toward a C=C bond to form an epoxy adduct and a nitrogen molecule. The reaction mechanisms are proposed to occur via the cyclic five-membered ring intermediate, called the stepwise mechanism (Subsection A) or via directly losing the O atom denoted in the concerted mechanism (Subsection B). The explanations of both mechanisms are clarified below.

A. Stepwise mechanism

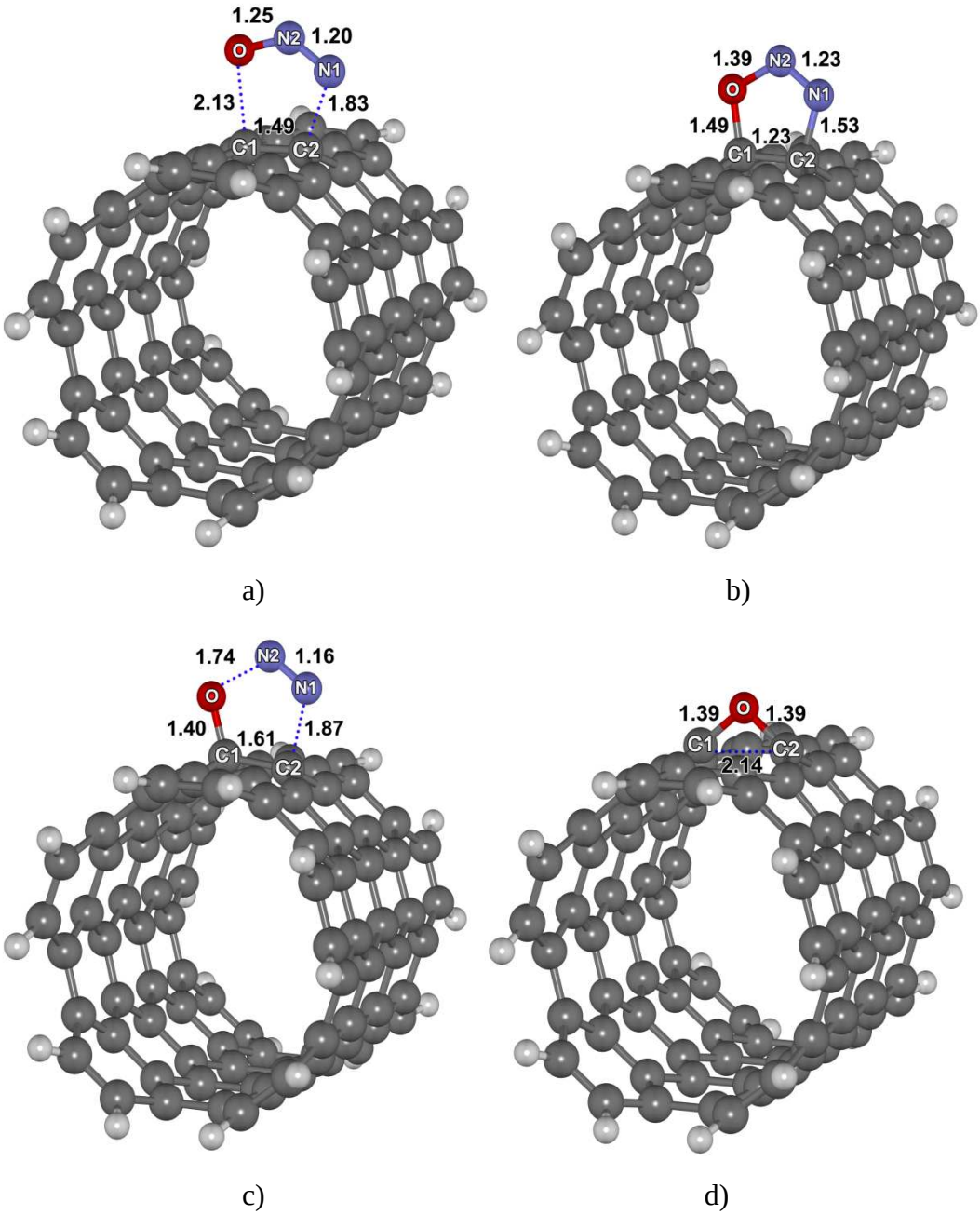

Figure 27 The reaction complexes associated with the stepwise mechanism for the decomposition of nitrous oxide to nitrogen on the perfect site of the armchair (5,5)-SWNT. (a) TS1p (37.23), (b) LM1p (25.31), (c) TS2p (35.97), and (d) LM2p (43.92). The values in parenthesis are the relative energies (in kcal/mol) of each individual complex with respect to the isolated molecules.

The stepwise mechanism of the nitrous oxide decomposition on the sidewall of SWNT is characterized by the formation of the cyclic intermediate. The complexes related to this mechanism are shown in Figure 27. At the initial step, the N_2O molecule approaches the C1–C2 in a parallel direction, and the reaction subsequently proceeds via two consecutive steps. The first step is an asynchronous cycloaddition forming a cyclic intermediate (LM1p). At the transition state (TS1p), the cycloaddition occurs via an electron transfer from C1–C2 of the SWNT to the N_2O molecule causing a lengthening of C1–C2 from 1.41 to 1.49 Å. Moreover, alterations in the N_2O structure are observed. The angle of ∠ON2N1 is bent from 180° to 137.8° owing to a hybridization change from sp (linear) to nearly sp^2 (bent). It is also confirmed by a lengthening of bond distances, which compare with the isolated N_2O molecule, by 0.06 Å for O–N2 and by 0.07 Å for N1–N2, which implies a weakening of those bonds in the N_2O molecule. Subsequently, after the cycloaddition process is completed, the metastable five-membered ring intermediate (LM1p) is formed with the adsorption energy of 25.31 kcal/ mol. The hybridizations of atoms in the N2O molecule are completely altered to sp^2. The O and N1 atoms are covalently bonded to C1 and C2 atoms with a single bond character (1.49 and 1.53 Å, respectively).

Lu and co-worker (2002c) studied the 1,3-dipolar cycloaddition of ozone (O_3) on an ONIOM2 model. Unlike a N_2O molecule, a symmetric O_3 molecule has a σ plane in between the left and right O-end atoms. Therefore, the reaction between O_3 and SWNT started from a synchronous cycloaddition with the σ_v symmetric transition state. The two forming C–O bonds are equivalent with a value of 2.29 Å. For the second step, the cyclic intermediate expels a nitrogen molecule and forms an epoxy adduct. At this point, the reaction proceeds via the second transition state (TS2p) where the N1–N2 shortens (1.16 Å) to form the nitrogen molecule simultaneously with the lengthening of O–N2 and N1–C2 to 1.74 and 1.87 Å, respectively.

At the final stage, the epoxy adduct is formed by complete expelling the nitrogen molecule. All processes require the activation energy 37.23 kcal/mol

relative to the isolated molecule. Figure 27 clearly shows that the cycloaddition in the first step is the rate-determining step for nitrous oxide decomposition on the perfect nanotube. Since the heterocyclic intermediate is unstable, extrusion of the N_2 molecule in the final step is more facile with a lower barrier of 10.66 kcal/mol with respect to the heterocyclic intermediate.

B. Concerted mechanism

Alternatively, the nitrous oxide decomposition on the sidewall of the perfect SWNT can proceed in a single step without forming the cyclic intermediate. This is called the concerted mechanism and its associated complexes are shown in Figure 28.

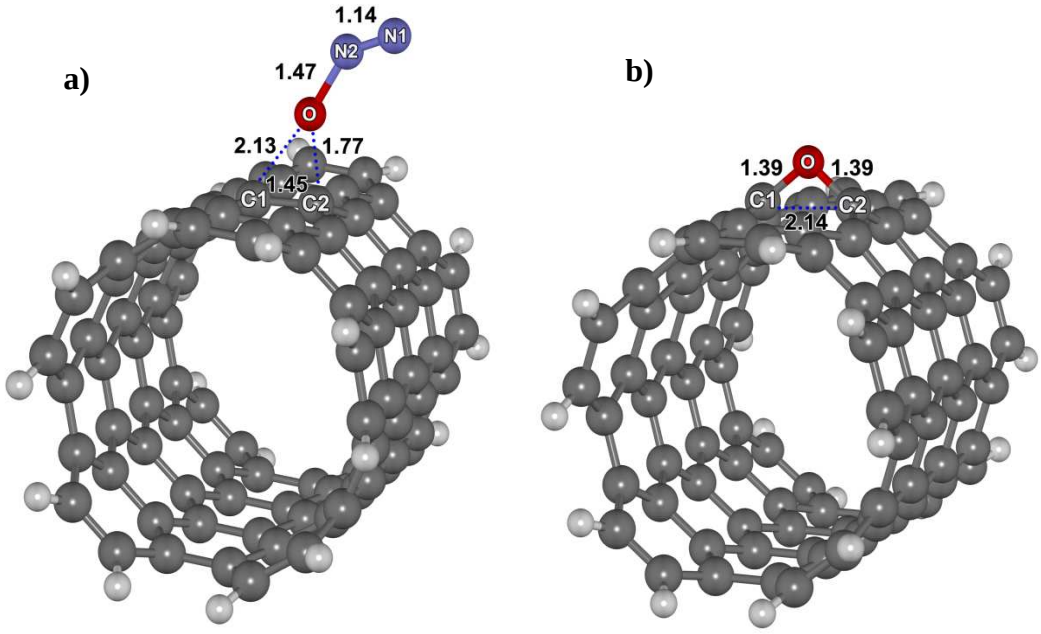

Figure 28 The reaction complexes associated with the concerted mechanism for the decomposition of nitrous oxide to nitrogen on the perfect site of the armchair (5,5)-SWNT. a) TSp (48.60), and (b) LM2p (-43.92). The values in parenthesis are the relative energies (in kcal/mol) of each individual complex with respect to the isolated molecules.

In the concerted mechanism, the reaction proceeds when an O atom approaches the C1–C2 bond and transfers an O atom to the tube creating the epoxy adduct. At the transition state (TSp), the O atom is pointing to the C1–C2 bond with nonequivalent O···C1 and O···C2 bond distances of 2.31 and 1.77 Å, respectively. In comparison to the isolated N_2O molecule, the O–N2 lengthens from 1.19 to 1.47 Å and N1–N2 shortens from 1.13 to 1.14 Å. The O–N2–N1 is changed from a linear to a bent alignment on account of the changing of the electronic hybridization of the central atom in the N_2O molecule. Finally, the product is also in the form of an epoxy adduct that is equivalent to that in the stepwise mechanism.

The calculated activation barrier for the concerted mechanism is 48.60 kcal/mol. In comparison with the stepwise mechanism, this concerted mechanism is relatively kinetically unfavorable. Therefore, it can be concluded that the stepwise mechanism is dominant and that the nitrous oxide favors to be decomposed on the sidewall of the perfect (5,5)-SWNT via the stepwise mechanism.

4.2 Reaction mechanisms on the Stone–Wales defect (5,5) SWNT

It is generally accepted that it is difficult to synthesize perfect nanotubes without defects, i.e. Stone–Wales defect, dopant, and vacancy (Charlier 2002). In this section, the role of the Stone–Wales (SW) defect on the reaction pathway is intend to examine by focusing on a 7–7 ring fusion site which is the same local bond center of the 1,2-pair site in the perfect model but it is rotated 90º. Even though the 7–7 ring fusion site is not the highest reactive site (Bettinger 2005, Lu *et al.*, 2005b), it was considered to be the important reactive centers for chemical adsorptions (Chakrapani *et al.*, 2003, Wang *et al.*, 2006) and reactions (Delgado *et al.*, 2004, Wang *et al.*, 2006, Wu *et al.*, 2006) on carbon nanotubes.

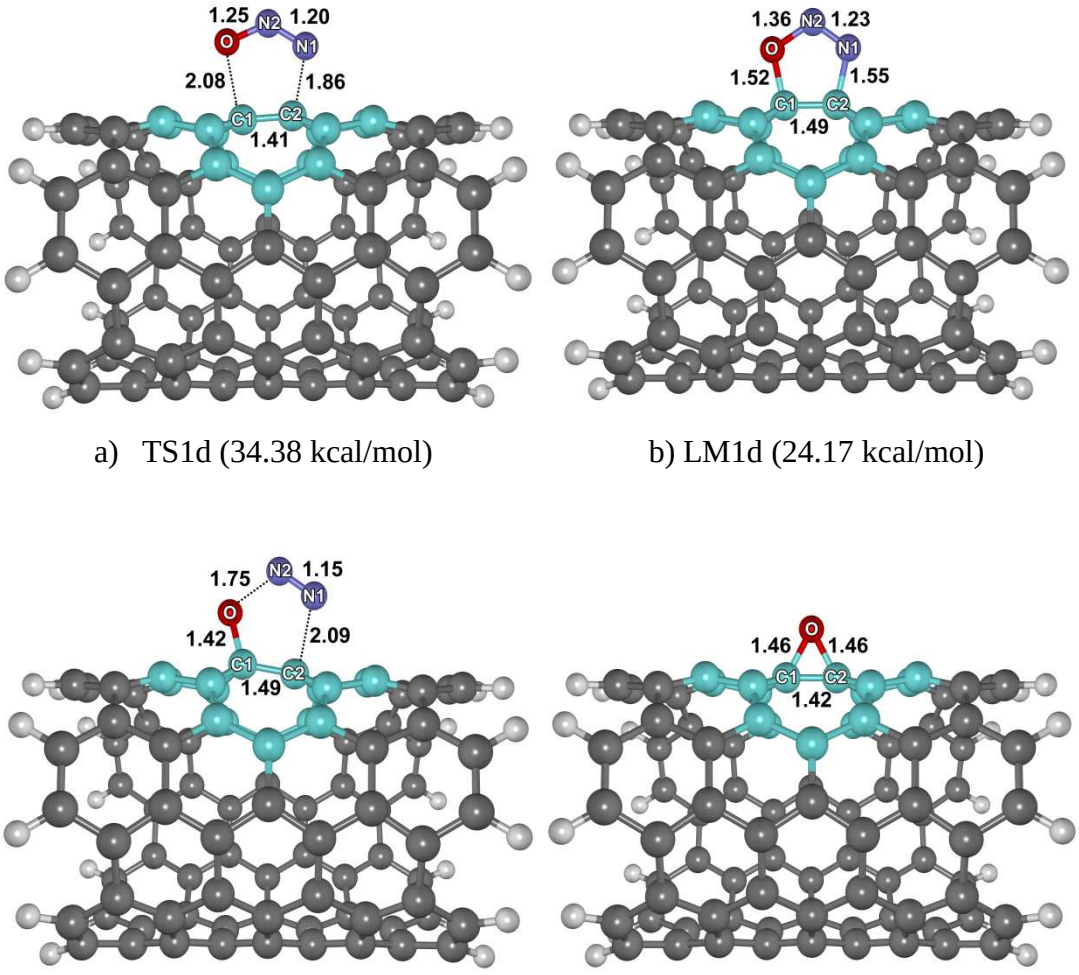

a) TS1d (34.38 kcal/mol) b) LM1d (24.17 kcal/mol)

c) TS2d (44.80 kcal/mol) d) LM2d (-30.56 kcal/mol)

Figure 29 The reaction complexes associated with the stepwise mechanism for the decomposition of nitrous oxide to nitrogen on the Stone–Wales defective site in the armchair (5,5)-pSWNT. The values in parenthesis are the relative energies of each individual complex with respect to the isolated molecules.

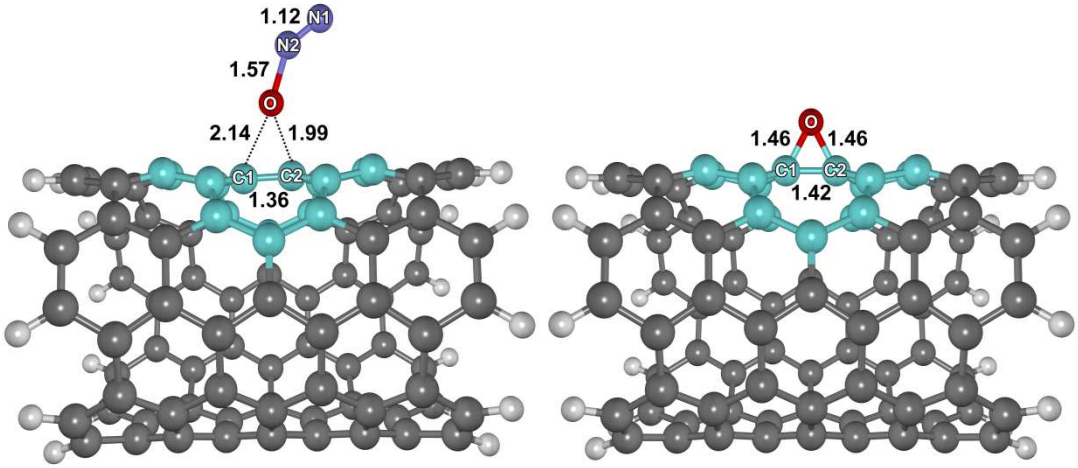

a) TSd (40.27 kcal/mol) b) LM2d (-30.56 kcal/mol)

Figure 30 The reaction complexes associated with the concerted mechanism for the decomposition of nitrous oxide to nitrogen on the Stone–Wales defective site in the armchair (5,5)-pSWNT. The values in parenthesis are the relative energies of each individual complex with respect to the isolated molecules.

Figures 29 and 30 show the optimized structure of all stationary points in the stepwise and concerted mechanisms for the decomposition of nitrous oxide at the 7–7 ring fusion of the Stone–Wales defect in (5,5)-SWNT (dSWNT). It is noted that the reaction mechanisms on the dSWNT are similar to those on the pSWNT (see Figures 27 and 28). However, some energy crossings occurred which are due mainly to the instability of the epoxy product on the dSWNT. For the cycloaddition step, the activation barrier of the dSWNT model is lower than that of the pSWNT model by 2.85 kcal/mol. In other words, the cycloaddition of N_2O to the dSWNT is more facilitative than to the pSWNT model. To characterize these results, the roles of N_2O and SWNT in the reaction is considered. In the decomposition process, the N_2O molecule acts as the electron deficiency molecule while the SWNT acts as the electron donating part. Thus, electrons will be transferred from the SWNT to N_2O in order to undergo the decomposition process. From the fact that the shorter the bond is, the higher the electron in the local bond is. Hence, the higher electron density in the C1–C2 bond of the dSWNT should aid the cycloaddition reaction with incoming N_2O.

Contrary to the cycloaddition step, the barrier height for the second step involving the nitrogen molecule extrusion to form an epoxy adduct in the dSWNT system is higher than that in the pSWNT by 8.83 kcal/mol. This can be explained by the Bell–Evans–Polyani Principle: the more the exothermic reaction is the lower the barrier height. In this case, the epoxy adduct of the pSWNT, in which the oxygen atom is attached to the circumferential C1–C2 bond, can release the strain by opening the epoxy ring leaving the opened form (see Figure 27d). For the dSWNT where the C1–C2 bond is in parallel with the tube, the epoxy ring forming via the axial addition is still in the closed form (see Figure 29d). These cause different relative energies and the more stable epoxy adduct in the pSWNT by 13.36 kcal/mol. In addition to the reaction energy, it is observed the stabilities of the epoxy adducts in terms of the binding energies of triplet O(t) atoms attached to the sidewalls of those nanotubes. The calculated O(t) binding energies on the pSWNT and the dSWNT are -91.32 and -77.96 kcal/mol, respectively. Our observations are in agreement with the Lu *et al.* work (Lu *et al.*, 2005b) that performed on the $C_{70}H_{20}$ model at the same level of theory. Their calculated additional energies are -74.6 and -62.4 kcal/mol for the pSWNT and the dSWNT systems, respectively. The differences in the values of their reaction energies and ours can be explained by the effect from edges in finite cluster calculations using their smaller model ($C_{70}H_{20}$). Moreover, based on Bettinger's and Matsuo's findings (Bettinger 2006, Matsuo *et al.*, 2003), the $C_{70}H_{20}$ tube model that possesses an incomplete Clar network is less reactive than the complete Clar network $C_{90}H_{20}$ model. However, in comparison to our results of 13.36 kcal/mol, this smaller model also estimates an energy difference of the two adducts by 12.2 kcal/mol on the potential energy surface.

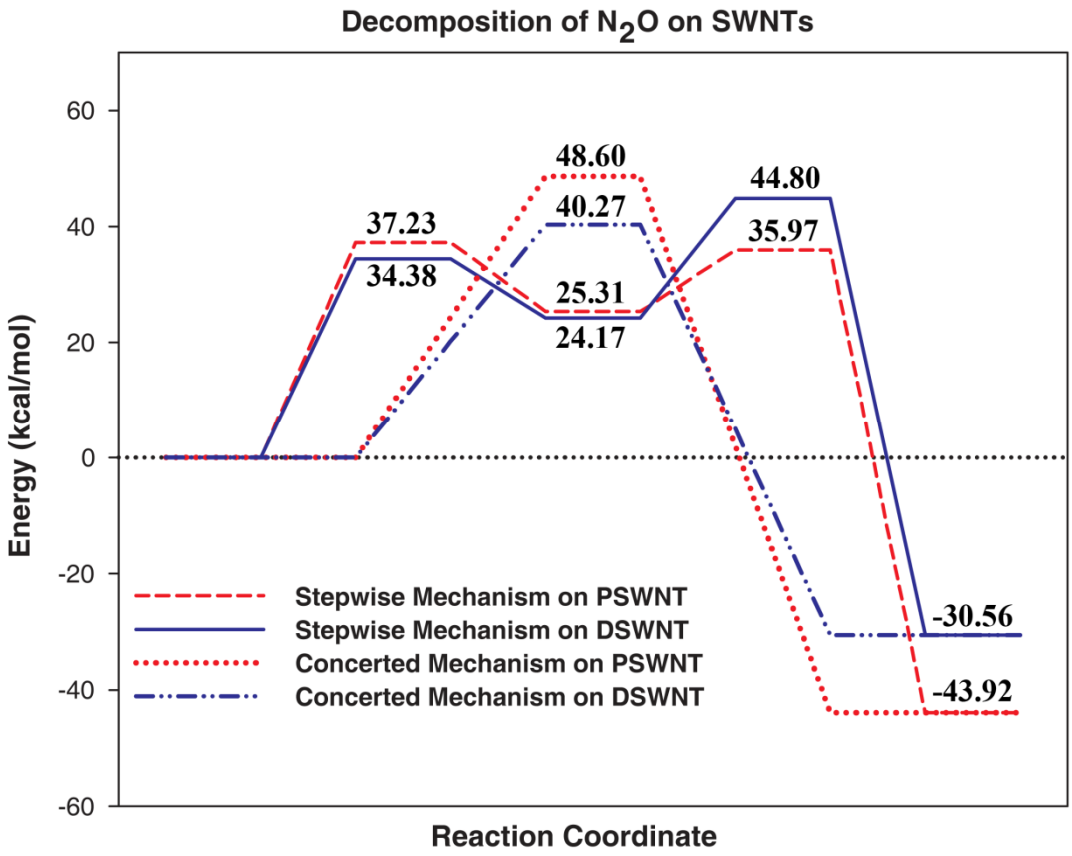

Figure 31 Energy profiles for the nitrous oxide decomposition on pSWNT and dSWNT fully optimized at B3LYP/6-31G(d).

4.3 Effect of Cl^-@SWNT on the reaction pathway

Since the activation energies of the decomposition of nitrous oxide on SWNT are rather high, in this section, a reduction of the barrier height of this reaction is studied. For the reason that the SWNT acts as a nucleophile, the introduction of an electron rich moiety into the SWNT might enhance its reactivity. As a case study, the chloride anion is doped into the SWNT (see Figure 12) by encapsulating it in the middle tube of the SWNT (Cl^-@SWNT). The whole reaction process was completed by single point calculations at every stationary point at the same level of theory.

Table 10 The relative and activation barrier energies regarding the N_2O decomposition on the bare perfect and the defective SWNTs and the Chloride anion doped perfect and the defective SWNTs.

SWNT	TS	TS1	LM1	TS2	LM2	O(t)	ΔEa_1	ΔEa_2
Bare								
Perfect	48.6	37.23	25.31	35.97	-43.92	-91.32	37.23	10.66
Defect	40.27	34.38	24.17	44.8	-30.56	-77.96	34.38	20.63
Cl^-@								
Perfect	44.5	32.21	20.94	31.21	-44.64	-92.03	32.21	10.27
Defect	38.34	32.13	23.82	41.76	-30.61	-78.00	32.13	17.93

Table 11 The charge gained on N_2O of all stationary points of N_2O decomposition on the bare perfect site (pSWNT), the defective site (dSWNT) and the Chloride anion doped perfect site (Cl^-@pSWNT), the defective site (Cl^-@dSWNT) of (5,5) SWNT.

	pSWNT	Cl^-@pSWNT	dSWNT	Cl^-@dSWNT
Stepwise				
TS1	-0.2797	-0.3561	-0.2724	-0.3538
LM1	-0.4196	-0.4764	-0.4076	-0.4647
TS2	-0.5544	-0.6144	-0.5696	-0.6398
LM2	-0.5576	-0.5723	-0.4759	-0.5123
Concerted				
TS	-0.2611	-0.4432	-0.2934	-0.3926

Using the explanation given in the Section 3.2, a certain relationship between a magnitude of electron gained on N_2O and the relative energy of the reaction complexes for the nitrous oxide decomposition are observed (see Tables 9 and 10). The relationship states that the higher the electron gained on N_2O, the lower the relative energy at every point in the reaction pathway. The barrier heights are decreased in the following order: Bare pSWNT > Cl^-@pSWNT and Bare dSWNT > Cl^-@dSWNT. These findings suggest that introducing an excess electron density onto the (5,5) armchair carbon nanotube can improve the reaction kinetics for decomposition of nitrous oxide onto the sidewall of SWNTs by enlarging the magnitude of the electron transfer from SWNTs to the N_2O molecule.

CONCLUSIONS

1. Adsorption of ethylene, benzene and ethylbenzene on faujasite zeolite

The adsorption of ethylene, benzene, and ethylbenzene on faujasite zeolite has been investigated with three different cluster sizes and methods comprising various two level ONIOM2 schemes. The bare 3T B3LYP/6-31G(d,p) quantum cluster approach predicts the adsorption energies of −8.14, −7.48, and −7.76 kcal/mol for ethylene, benzene, and ethylbenzene, respectively. The effect of the zeolite framework is modeled on the ONIOM2 method. The extended framework is found to significantly enhance their adsorption energy of adsorbates to the zeolites. In particular, the final predicted adsorption energies of −8.75, −15.17, and −21.08 kcal/mol, for the ethylene, benzene, and ethylbenzene adsorption complexes were calculated by the ONIOM2(B3LYP/6-311++G(d,p):UFF) scheme. This efficient scheme performs superbly when compared with the experimental estimates of −9.1, −15.3, and −19.6 kcal/mol, respectively. The results obtained in this study suggest that the ONIOM approach yields a more accurate and practical model in studying the adsorption of unsaturated hydrocarbons on zeolites.

2. Alkylation of benzene with ethylene and dimerization of ethylene

The alkylation of benzene with ethylene and dimerization of ethylene over faujasite zeolite have been investigated using the ONIOM3 model. The model is shown to be accurate in predicting adsorption energies of the adsorbed reactants and products compared to experimental estimates. Two mechanisms, stepwise and concerted, have been evaluated for both reactions. For the stepwise mechanism, both reactions start with the same step of protonation of the adsorbed ethylene which leads to the formation of the active surface ethoxide intermediate with the barrier of 30.06 kcal/mol. For the second step, benzene alkylation takes place via interactions between the ethoxide species and a benzene molecule. The rate-determining step is found to be the reaction step where concerted bond forming between the carbon of the ethyl fragment and benzene and bond breaking of a benzene proton occur. The activation

energy of 38.18 kcal/mol is predicted. Alternatively, dimerization of ethylene, the active surface ethoxide intermediate can form C-C bond with the second ethylene molecule with the activation energy of 28.87 kcal/mol, slightly lower than the rate-determining step of benzene alkylation (30.06 kcal/mol).

For the concerted mechanism, the alkylation of benzene takes place in a single reaction step of the co-adsorbed reactants without prior alkoxide formation. The activation energy is calculated to be 33.41 kcal/mol. Like benzene alkylation, protonation and C-C bond formation of ethylene dimerization occur simultaneously at one transition state to form butoxy adduct. The activation barrier of the concerted mechanism (38.08 kcal/mol) is higher than that of the rate-determining step of the stepwise mechanism (30.06 kcal/mol). Therefore, for ethylene dimerization, the stepwise mechanism occurs faster than the concerted mechanism.

3. Structures and reaction mechanisms of propene oxide isomerization

The isomerization of propene oxide over 5T and 46T clusters of H-ZSM-5 zeolite has been investigated by using the B3LYP/6-31G(d,p) and ONIOM(B3LYP/6-31G(d,p): UFF) methods. The reaction mechanisms proceed through a ring-opening step followed by a 1,2-hydride shift to form two different carbonyl compounds, propanal and propanone. The ring-opening step of these mechanisms is found to be the rate-determining step and their transition states are in the carbenium ion form. The propanal route proceeds via the secondary carbenium ion while that of the propanone proceeds via the primary one. Because the sterically more hindered C-O bond can be broken more easily and the secondary carbenium ion transition state is more stable, the ring-opening activation barrier for the propanal of 38.5 kcal/mol is lower than that for the propanone of 42.4 kcal/mol. The main product from this reaction is, therefore, the propanal.

The computational results suggest that the 5T cluster is adequate to determine the geometrical characters of the transition state, the intermediate, the reactant, and the product of these small adsorbates. However, since the 5T cluster does not take into

account the van der Waals from the zeolite framework, it cannot give reasonable results for the energetic profile of the reaction. The extended 46T ONIOM model, which includes the zeolite cavity and those effects, can be used to calculate more reliable results.

4. Carbon Nanotubes: Decomposition of nitrous oxide

The decomposition of a nitrous oxide molecule on the sidewall of the perfect- and the Stone–Wales defect (5,5)-SWNTs have been studied from the first principle calculations. The predicted reaction mechanisms (the stepwise and concerted mechanisms) are analogous for the perfect and the defective models. For the stepwise mechanism, the reaction occurs through a cyclic intermediate via an asynchronous cycloaddition and followed by the extrusion of a nitrogen molecule. The activation barrier for the rate-determining cycloaddition step is calculated to be 37.23 kcal/mol for the perfect and 34.38 kcal/mol for the defective models, respectively. The five-membered ring complex is an unstable intermediate and results a low activation barrier in the final step (10.66 kcal/mol for the perfect and 20.63 kcal/mol for the defective models, respectively). For the concerted mechanism, the nitrous oxide molecule directly transfers an O atom to the SWNT in a single step. The activation barriers are evaluated to be 48.60 kcal/mol for the perfect and 40.27 kcal/mol for the defective models, respectively. The reaction barriers in the concerted mechanism are higher than those in the stepwise mechanism. Therefore, it is concluded that the nitrous oxide molecule can be decomposed favorably on the armchair (5,5)-SWNT via the stepwise mechanism.

The effect of a chloride anion encapsulated into the SWNTs has also been studied. It is clearly demonstrated that the presence of the chloride anion inside the channel of the SWNTs increases the catalytic reactivity of the SWNTs for the nitrous oxide decomposition on the perfect and the Stone–Wales defect SWNTs by enhancing the electron transfer from the tube to the N_2O molecule. Although the calculated smallest barrier for these systems (34.38 kcal/mol) is rather high, this study would assist the experimentalists in fine-tuning an effective condition of further explorations

which may lead to a new efficient process for the removal of toxic N_2O gas in the future.

In summary, the nanostructured zeolites, faujasite and ZSM-5, which are the catalysts in the important reactions studied above can be modeled with the clusters and represented by ONIOM methods. Faujasite zeolite consisting of 576 atoms in unit cell, can be modeled by 84T cluster and successfully used to represent the interactions between the zeolite's active site, surrounded with environmental framework, and the upcoming adsorbed molecules by using both ONIOM2(B3LYP/6-311++G**:UFF) and ONIOM3(MP2/6-311++G**:HF/6-31G*:UFF) methods. Whereas, smaller unit cell of ZSM-5 consisting of 297 atoms can be designed by using even small cluster of 46 tetrahedral atoms and treated with ONIOM2(B3LYP/6-31G**:UFF) method. These models and methods are then used to investigate the reaction mechanims catalyzed by zeolites, i.e. the alkylation of benzene with ethylene, the dimerization of ethylene, and the isomerization of propene oxide to carbonyl compounds. The most importantly, the behaviours of small atoms and molecules on the active site can be understood in molecular level, let one can design the new/better catalysts for their interested reactions.

LITERATURE CITED

Al-Baghli, N., S. Al-Khattaf and P.N. J. Cejka. 2005. Catalytic cracking of a mixture of dodecane and 1,3,5 triisopropyl-benzene over USY and ZSM-5 zeolites based catalysts. **Stud. Surf. Sci. Catal.** 158(2): 1661-1668.

Arstad, B., S. Kolboe and O. Swang. 2004. Theoretical investigation of arene alkylation by ethene and propene over acidic zeolites. **J. Phys. Chem. B** 108(7): 2300-2308.

Avouris, P. 2002. Molecular electronics with carbon nanotubes. **Acc. Chem. Res.** 35(12): 1026-1034.

Barthomeuf, D. and B.H. Ha. 1973. Adsorption of benzene and cyclohexane on faujasite-type zeolites. **J. Chem. Soc., Faraday Trans.** 69(12): 2147.

Beck, W., T. Xu, J.B. Nicholas and J.F. Haw. 1995. Kinetic NMR and density functional study of benzene H/D exchange in zeolites, the most simple aromatic substitution. **J. Am. Chem. Soc.** 117(46): 11594-11595.

Becke, A.D. 1993. Density-functional thermochemistry. III. The role of exact exchange**. J. Chem. Phys.** 98(7): 648-5652.

Becker, K.A., H.G. Karge and W.D. Streubel. 1973. Benzene alkylation with ethylene and propylene over H-mordenite as catalyst. **J. Catal.** 28:403-413.

Bellussi, G., G. Pazzuconi, C. Perego, G. Girotti and G. Terzoni. 1995. Liquid-phase alkylation of benzene with light olefins catalyzed by b zeolites. **J. Catal.** 157(1): 227-234.

Bettinger, H.F. 2004. Effects of finite carbon nanotube length on sidewall addition of fluorine atom and methylene. **Org. Lett.** 6(5): 731-734.

_____. 2005. The reactivity of defects at the sidewalls of single-walled carbon nanotubes: The stone-wales defect. **J. Phys. Chem. B** 109(15): 6922-6924.

_____. 2006. Addition of carbenes to the sidewalk of single-walled carbon nanotubes. **Chem-Eur. J.** 12(16): 4372-4379.

Bibby, D.M., R.F. Howe and G.D. McLellan. 1992. Coke formation in high-silica zeolites. **Appl. Catal.** 93:1-34.

Bobuatong, K. and J. Limtrakul. 2003. Effects of the zeolite framework on the adsorption of ethylene and benzene on alkali-exchanged zeolites: An ONIOM study. **Appl. Catal. A** 253(1): 49-64.

Boronat, M., P. Viruela and A. Corma. 1998. A theoretical study of the mechanism of the hydride transfer reaction between alkanes and alkenes catalyzed by an acidic zeolite. **J. Phys. Chem. A** 102(48): 9863-9868.

_____, C. M. Zicovich-Wilson, P. Viruela, A. Corma. 2001. Influence of the Local Geometry of Zeolite Active Sites and Olefin Size on the Stability of Alkoxide Intermediates. J. Phys. Chem. B 105(45): 11169-11177.

_____, C. M. Zicovich-Wilson, P. Viruela, A. Corma. 2001. Influence of the local geometry of zeolite active sites and olefin size on the stability of alkoxide intermediates. **J. Phys. Chem. B** 105(45): 11169-11177.

_____, P.M. Viruela and A. Corma. 2004. Reaction Intermediates in Acid Catalysis by Zeolites: Prediction of the Relative Tendency to Form Alkoxides or Carbocations as a Function of Hydrocarbon Nature and Active Site Structure. **J. Am. Chem. Soc.** 126(10): 3300-3309.

Braendle, M. and J. Sauer. 1998. Acidity differences between inorganic solids induced by their framework structure. A combined quantum

mechanics/molecular mechanics ab initio study on zeolites. **J. Am. Chem. Soc.** 120(7): 1556-1570.

Brand, H.V., L.A. Curtiss and L.E. Iton. 1993. Ab initio molecular orbital cluster studies of the zeolite ZSM-5. 1. Proton affinities. **J. Phys. Chem.** 97(49): 12773-12782.

Cant, N.W. and W.K. Hall. 1972. Studies of the hydrogen held by solids: XXI. The interaction between ethylene and hydroxyl groups of a Y-zeolite at elevated temperatures. **J. Catal.** 25(1):161-172.

Carlier, P.R. 2004. Threading the needle: Mimicking natural toroidal catalysts. **Angew. Chem. Int. Edit.** 43(20): 2602-2605.

_____, N. Deora and T.D. Crawford. 2006. Protonated 2-methyl-1,2-epoxypropane: A challenging problem for density functional theory. **J. Org. Chem.** 71(4): 1592-1597.

Centi, G. and F. Vazzana. 1999. Selective catalytic reduction of N_2O in industrial emissions containing O_2, H_2O and SO_2: Behavior of Fe/ZSM-5 catalysts. **Catal. Today** 53(4): 683-693.

Chakrapani, N., Y.M. Zhang, S.K. Nayak, J.A. Moore, D.L. Carroll, Y.Y. Choi and P.M. Ajayan. 2003. Chemisorption of acetone on carbon nanotubes. **J. Phys. Chem. B** 107(35): 9308-9311.

Charlier, J.C. 2002. Defects in carbon nanotubes. **Acc. Chem. Res.** 35(12): 1063-1069.

Chen, N.Y. and W.E. Garwood. 1986. Industrial application of shape-selective catalysis. **Catal. Rev.** 28(2-3): 185-264.

Cheng, J. C., T.F. Degnan, J.S. Beck, Y.Y. Huang, M. Kalyanaraman, J.A. Kowalski, C.A. Loehr and D.N. Mazzone. 1999. A comparison of zeolites MCM-22,

Beta, and USY for liquid phase alkylation of benzene with ethylene. **Stud. Surf. Sci. Catal.** 121: 53-60.

Cheng, Z., X. Zhu, G.D. Fu, E.T. Kang and K.G. Neoh. 2005. Dual-brush-type amphiphilic triblock copolymer with intact epoxide functional groups from consecutive RAFT polymerizations and ATRP. **Macromolecules** 38(16): 7187-7192.

Christoforou, S.C., E.A. Efthimiadis and I.A. Vasalos. 2002. Catalytic conversion of N_2O to N_2 over metal-based catalysts in the presence of hydrocarbons and oxygen. **Catal. Lett.** 79(1-4): 137-147.

Chu, Y.Y. and M.D. Su. 2004. Theoretical study of addition reactions of carbene, silylene, and germylene to carbon nanotubes. **Chem. Phys. Lett.** 394(4-6): 231-237.

Clark, L.A., M. Sierka and J. Sauer. 2003. Stable mechanistically-relevant aromatic-based carbenium ions in zeolite catalysts. **J. Am. Chem. Soc.** 125(8): 2136-2141.

Coker, E.N., C. Jia and H.G. Karge. 2000. Adsorption of benzene and benzene derivatives onto zeolite H-Y studied by microcalorimetry. **Langmuir** 16(3): 1205-1210.

Corma, A. 1995. Inorganic solid acids and their use in acid-catalyzed hydrocarbon reactions. **Chem. Rev.** 95(3): 559-614.

_____, V. Martinez-Soria and E. Schnoeveld. 2000. Alkylation of benzene with short-chain olefins over MCM-22 zeolite: Catalytic behaviour and kinetic mechanism. **J. Catal.** 192(1): 163-173.

Correa, R.J. and C.J.A. Mota. 2002. Theoretical study of protonation of butene isomers on acidic zeolite: The relative stability among primary, secondary and tertiary alkoxy intermediates. **Phys. Chem. Chem. Phys.** 4(2): 375-380.

Coxon, J.M., R.G.A.R. Maclagan, A. Rauk, A.J. Thorpe and D. Whalen. 1997. Rearrangement of protonated propene oxide to protonated propanal. **J. Am. Chem. Soc.** 119(20): 4712-4718.

_____, A.J. Thorpe and W.B. Smith. 1999. Potential energy surface for the acid- and BF3-catalyzed rearrangement of methylpropene oxide. **J. Org. Chem.** 64(26): 9575-9586.

Dapprich, S., I. Komaromi, K.S. Byun, K. Morokuma and M.J. Frisch. 1999. A new ONIOM implementation in Gaussian98. Part I. The calculation of energies, gradients, vibrational frequencies and electric field derivatives. **J. Mol. Struct.-THEOCHEM** 461-462: 1-21.

Degnan Jr, T.F., C.M. Smith and C.R. Venkat. 2001. Alkylation of aromatics with ethylene and propylene: Recent developments in commercial processes. **Appl. Catal. A** 221(1-2): 283-294.

Dekker, C. 1999. Carbon nanotubes as molecular quantum wires. **Phys. Today** 52(5): 22-28.

Delgado, J.L., P. De La Cruz, F. Langa, A. Urbina, J. Casado and J.T. Lopez Navarrete. 2004. Microwave-assisted sidewall functionalization of single-wall carbon nanotubes by Diels-Alder cycloaddition. **Chem. Commun.** 10(15): 1734-1735.

Derouane, E.G. and C.D. Chang. 2000. Confinement effects in the adsorption of simple bases by zeolites. **Micropor. Mesopor. Mat.** 35-36: 425-433.

Dewar, M.J.S., W. Theil. 1997. Ground states of molecules. 39. MNDO results for molecules containing hydrogen, carbon, nitrogen, and oxygen. **J. Am. Chem. Soc.** 99(15): 4907-4917.

Dimitrova, R., V. Minkov and N. Micheva. 1996. Zeolite catalyzed ring opening of styrene oxide. **Appl. Catal. A** 145(1-2): 49-55.

Du, Y., H. Wang and S. Chen. 2002. Study on alkylation of benzene with ethylene over beta zeolite catalyst to ethylbenzene by in situ IR. **J. Mol. Catal. A** 179(1-2): 253-261.

Evleth, E.M., E. Kassab, H. Jessri, M. Allavena, L. Montero and L.R. Sierra. 1996. Calculation of the reaction of ethylene, propene, and acetylene on zeolite models. **J. Phys. Chem.** 100(27): 11368-11374.

Fasi, A., A. Gomory, I. Palinko and I. Kiricsi. 2001. Isomerization and dimerization reactions of methyloxirane over various types of zeolite and zeotype. **J. Catal.** 200(2): 340-344.

_____, I. Palinko, A. Gomory and I. Kiricsi. 2004. Ring opening, dimerisation and oligomerisation reactions of methyloxirane on solid acid and base catalysts. **J. Mol. Catal. A** 208(1-2): 307-311.

Frash, M. V., V.B. Kazansky, A.M. Rigby and R.A. van Santen. 1998. Cracking of hydrocarbons on zeolite catalysts: density functional and Hartree-Fock calculations on the mechanism of the β-Scission Reaction. **J. Phys. Chem. B** 102(12): 2232-2238.

Flego, C., I. Kiricsi, C. Perego and G. Bellussi. 1995. Adsorption of propene, benzene, their mixtures and cumene on H-beta zeolites studied by IR and UV-VIS Spectroscopy. **Stud. Surf. Sci. Catal.** 94: 405-412.

Freude, D., J. Klinowski and H. Hamdan. 1988. Solid-state NMR studies of the geometry of brønsted acid sites in zeolitic catalysts. **Chem. Phys. Lett.** 149(4): 355-362.

Frisch, M.J., G.W. Trucks, H.B. Schlegel, P.M.W. Gill, B.G. Johnson, M.A. Robb, J.R. Cheeseman, T. Keith, G.A. Petersson, J.A. Montgomery, K. Raghavachari, M.A. Al-Laham, V.G. Zakrzewski, J.V. Ortiz, J.B. Foresman, J. Cioslowski, B.B. Stefanov, A. Nanayakkara, M. Challacombe, C.Y. Peng, P.Y. Ayala, W. Chen, M.W. Wong, J.L. Andres, E.S. Replogle, R. Gomperts,

R.L. Martin, D.J. Fox, J.S. Binkley, D.J. Defrees, J. Baker, J.P. Stewart, M. Head-Gordon, C. Gonzalez and J.A. Pople. 2001. Gaussian 98.

_____, G.W. Trucks, H.B. Schlegel, G.E. Scuseria, M.A. Robb, J.R. Cheeseman, J. Montgomery, J. A., T. Vreven, K.N. Kudin, J.C. Burant, J.M. Millam, S.S. Iyengar, J. Tomasi, V. Barone, B. Mennucci, M. Cossi, G. Scalmani, N. Rega, G.A. Petersson, H. Nakatsuji, M. Hada, M. Ehara, K. Toyota, R. Fukuda, J. Hasegawa, M. Ishida, T. Nakajima, Y. Honda, O. Kitao, H. Nakai, M. Klene, X. Li, J.E. Knox, H.P. Hratchian, J.B. Cross, V. Bakken, C. Adamo, J. Jaramillo, R. Gomperts, R.E. Stratmann, O. Yazyev, A.J. Austin, R. Cammi, C. Pomelli, J.W. Ochterski, P.Y. Ayala, K. Morokuma, G.A. Voth, P. Salvador, J.J. Dannenberg, V.G. Zakrzewski, S. Dapprich, A.D. Daniels, M.C. Strain, O. Farkas, D.K. Malick, A.D. Rabuck, K. Raghavachari, J.B. Foresman, J.V. Ortiz, Q. Cui, A.G. Baboul, S. Clifford, J. Cioslowski, B.B. Stefanov, G. Liu, A. Liashenko, P. Piskorz, I. Komaromi, R.L. Martin, D.J. Fox, T. Keith, M.A. Al-Laham, C.Y. Peng, A. Nanayakkara, M. Challacombe, P.M.W. Gill, B. Johnson, W. Chen, M.W. Wong, C. Gonzalez and J.A. Pople. 2004. Gaussian 03.

Geobaldo, F., G. Spoto, S. Bordiga, C. Lamberti and A. Zecchina. 1997. Propene oligomerization on H-mordenite: Hydrogen-bonding interaction, chain initiation, propagation and hydrogen transfer studied by temperature-programmed FTIR and UV-VIS spectroscopies. **J. Chem. Soc., Faraday Trans.** 6: 1243-1249.

Georgakilas, V., K. Kordatos, M. Prato, D.M. Guldi, M. Holzinger and A. Hirsch. 2002. Organic functionalization of carbon nanotubes. **J. Am. Chem. Soc.** 124(5): 760-761.

George, P., C.W. Bock and J.P. Glusker. 1992. Protonation of monosubstituted oxiranes: A computational molecular orbital study of oxonium ion versus carbonium ion formation. **J. Phys. Chem.** 96(9): 3702-3708.

Gomez, B., J.M. Martinez-Magadan, U. Sarkar and P.K. Chattaraj. 2005. Cracking of n-heptane in HZSM-5 zeolite. **J. Mol. Struct.-THEOCHEM** 755(1-3): 99-103.

Greatbanks, S.P., I.H. Hillier, N.A. Burton and P. Sherwood. 1996. Adsorption of water and methanol on zeolite Brønsted acid sites: An ab initio, embedded cluster study including electron correlation. **J. Chem. Phys.** 105(9): 3770-3776.

Haw, J.F., B.R. Richardson, I.S. Oshiro, N.D. Lazo and J.A. Speed. 1989. Reaction of propene on zeolite HY catalyst studied by in situ variable-temperature solid-state nuclear magnetic resonance spectroscopy. **J. Am. Chem. Soc.** 111: 2052-2058.

Helten, H., T. Schirmeister and B. Engels. 2004. Model calculations about the influence of protic environments on the alkylation step of epoxide, aziridine, and thiirane based cysteine protease inhibitors. **J. Phys. Chem. A** 108(38): 7691-7701.

_____, T. Schirmeister and B. Engels. 2005. Theoretical studies about the influence of different ring substituents on the nucleophilic ring opening of three-membered heterocycles and possible implications for the mechanisms of cysteine protease inhibitors. **J. Org. Chem.** 70(1): 233-237.

Hill, J.R., C.M. Freeman and B. Delley. 1999. Bridging hydroxyl groups in faujasite: Periodic vs cluster density functional calculations. **J. Phys. Chem. A** 103(19): 3772-3777.

Hillier, I.H. 1999. Chemical reactivity studied by hybrid QM/MM methods. **J. Mol. Struct.-THEOCHEM** 463(1-2): 45-52.

Holzinger, M., J. Steinmetz, D. Samaille, M. Glerup, M. Paillet, P. Bernier, L. Ley and R. Graupner. 2004. [2+1] Cycloaddition for cross-linking SWCNTs. **Carbon** 42(5-6): 941-947.

Hsia Chen, C.S. and R.F. Bridger. 1996. Shape-selective oligomerization of alkenes to near-linear hydrocarbons by zeolite catalysis. **J. Catal.** 161(2): 687-693.

Hu, H., B. Zhao, M.A. Hamon, K. Kamaras, M.E. Itkis and R.C. Haddon. 2003. Sidewall Functionalization of Single-Walled Carbon Nanotubes by Addition of Dichlorocarbene. **J. Am. Chem. Soc.** 125(48): 14893-14900.

Jeong, S., K.J. Fisher, R.F. Howe and G.D. Willett. 1998. A Fourier transform mass spectrometry study of ethene oligomers in HMFI zeolite. **Micropor. Mesopor. Mat.** 22(1-3): 369-377.

Jin Y. and C. Hao. 2005. Computational Study of the Stone-Wales Transformation in C_{36}. **J. Phys. Chem. A** 109; 2875-2877.

Joshi, Y.V. and K.T. Thomson. 2005. Embedded cluster (QM/MM) investigation of C6 diene cyclization in HZSM-5. **J. Catal.** 230(2): 440-463.

Kaeding, W.W. and R.E. Holland. 1988. Shape-selective reactions with zeolite catalysts: VI. Alkylation of benzene with propylene to produce cumene. **J. Catal.** 109(1): 212-216.

Kapteijn, F., J. Rodriguez-Mirasol and J.A. Moulijn. 1996. Heterogeneous catalytic decomposition of nitrous oxide. **Appl. Catal. B** 9(1-4): 25-64.

Kasuriya, S., S. Namuangruk, P. Treesukol, M. Tirtowidjojo and J. Limtrakul. 2003. Adsorption of ethylene, benzene, and ethylbenzene over faujasite zeolites investigated by the ONIOM method. **J. Catal.** 219(2): 320-328.

Katsuki, T. and K.B. Sharpless. 1980. The first practical method for asymmetric epoxidation. **J. Am. Chem. Soc.** 102(18): 5974-5976.

Kawasaki, S., K. Komatsu, F. Okino, H. Touhara and H. Kataura. 2004. Fluorination of open- and closed-end single-walled carbon nanotubes. **Phys. Chem. Chem. Phys.** 6(8): 1769-1772.

Kazanskii, V. B., and I.N. Senchenya. 1992. The real nature of aliphatic carbenium ions as active intermediates of homogeneous and heterogeneous acid catalysis. **J. Mol. Catal.** 74(1-3): 257-66.

_____. Adsorbed carbocations as transition states in heterogeneous acid catalyzed transformations of hydrocarbons. 1999. **Catal. Today** 51(3-4): 419-434.

Khaliullin, R.Z., A.T. Bell and V.B. Kazansky. 2001. An experimental and density functional theory study of the interactions of CH_4 with H-ZSM-5. **J. Phys. Chem. A** 105(45): 10454-10461.

Kiricsi, I., H. Forster, G. Tasi and J.B. Nagy. 1999. Generation, Characterization, and Transformations of Unsaturated Carbenium Ions in Zeolites. **Chem. Rev.** 99(8): 2085-2114.

Klepel, O., A. Loubentsov, W. Bohlmann and H. Papp. 2003. Oligomerization as an important step and side reaction for skeletal isomerization of linear butenes on H-ZSM-5. **Appl. Catal. A** 255(2): 349-354.

Knifton, J.F., J.R. Sanderson and P.E. Dai. 1994. Olefin oligomerization via zeolite catalysis. **Catal. Lett.** 28(2-4): 223-230.

Lau, E.Y., Z.E. Newby and T.C. Bruice. 2001. A theoretical examination of the acid-catalyzed and noncatalyzed ring-opening reaction of an oxirane by nucleophilic addition of acetate. Implications to epoxide hydrolases. **J. Am. Chem. Soc.** 123(14): 3350-3357.

Lebedev, N.G., I.V. Zaporotskova and L.A. Chernozatonskii. 2003. Fluorination of carbon nanotubes: Quantum chemical investigation within MNDO approximation. **Int. J. Quantum Chem.** 96(2): 142-148.

Lee, C., W. Yang and R.G. Parr. 1988. Development of the Colle-Salvetti correlation-energy formula into a functional of the electron density. **Phys. Rev. B** 37(2): 785-789.

Lesthaeghe, D., V. Van Speybroeck, G.B. Marin and M. Waroquier. 2005. DFT investigation of alkoxide vs alkylammonium formation in amine-substituted zeolites. **J. Phys. Chem. B** 109(16): 7952-7960.

Li, R., Z. Shang, G. Wang, Y. Pan, Z. Cai and X. Zhao. 2002. Study on dichlorocarbene cycloaddition isomers of armchair single-walled carbon nanotubes. **J. Mol. Struct.-THEOCHEM** 583: 241-247.

Limtrakul, J., S. Jungsuttiwong and P. Khongpracha. 2000. Adsorption of carbon monoxide on H-FAU and LI-FAU zeolites: An embedded cluster approach. **J. Mol. Struct.** 525(1-3): 153-162.

Liu, L.V., W.Q. Tian and Y.A. Wang. 2006. Ozonization at the vacancy defect site of the single-walled carbon nanotube. **J. Phys. Chem. B** 110(26): 13037-13044.

Long, L., X. Lu, F. Tian and Q. Zhang. 2003. Hydroboration of C(100) surface, fullerene, and the sidewalls of single-wall carbon nanotubes with borane. **J. Org. Chem.** 68(11): 4495-4498.

Lu, J., S. Nagase, X. Zhang, Y. Maeda, T. Wakahara, T. Nakahodo, T. Tsuchiya, T. Akasaka, D. Yu, Z. Gao, R. Han and H. Ye. 2005a. Structural evolution of [2+1] cycloaddition derivatives of single-wall carbon nanotubes: From open structure to closed three-membered ring structure with increasing tube diameter. **J. Mol. Struct.-THEOCHEM** 725(1-3): 255-257.

Lu, X., Z. Chen and P.V.R. Schleyer. 2005b. Are stone-wales defect sites always more reactive than perfect sites in the sidewalls of single-wall carbon nanotubes? **J. Am. Chem. Soc.** 127(1): 20-21.

_____, F. Tian, N. Wang and Q. Zhang. 2002a . Organic functionalization of the sidewalls of carbon nanotubes by Diels-Alder reactions: A theoretical prediction. **Org. Lett.** 4(24): 4313-4315.

_____, X. Xu, N. Wang and Q. Zhang. 2002b. A DFT study of the 1,3-dipolar cycloadditions on the C(100)-2 × 1 surface. **J. Org. Chem.** 67(2): 515-520.

_____, L. Zhang, X. Xu, N. Wang and Q. Zhang. 2002c. Can the sidewalls of single-wall carbon nanotubes be ozonized? **J. Phys. Chem. B** 106(9): 2136-2139.

_____, L. Zhang, X. Xu, N. Wang and Q. Zhang. 2003a. A theoretical exploration of the 1,3-dipolar cycloadditions onto the sidewalls of (n,n) armchair single-wall carbon nanotubes. **J. Am. Chem. Soc.** 125(34): 10459-10464.

_____, L. Zhang and Q. Zhang. 2003b. The [2+1] cycloadditions of dichlorocarbene, silylene, germylene, and oxycarbonylnitrene onto the sidewall of armchair (5,5) single-wall carbon nanotube. **J. Phys. Chem. B** 107(33): 8388-8391.

Martins, A., J.M. Silva, F.R. Ribeiro, M.F. Ribeiro and N.Z.a.P.N. J. Cejka. 2005. Isomerization of n-hexane on bifunctional catalysts Pt/HBEA and Pt/HMCM-22 with rare earth elements. **Stud. Surf. Sci. Catal.** 158(2): 1875-1882.

Maseras, F and K. Morokuma. 1995. IMOMM: A new integrated ab initio + molecular mechanics geometry optimization scheme of equilibrium structures and transition states. **J. Comp. Chem.** 16(9):1170–1179.

Matsuo, Y., K. Tahara and E. Nakamura. 2003. Theoretical studies on structures and aromaticity of finite-length armchair carbon nanotubes. **Org. Lett.** 5(18): 3181-3184.

Miyamoto, Y., N. Jinbo, H. Nakamura, A. Rubio and D. Tomanek. 2004. Photodesorption of oxygen from carbon nanotubes. **Phys. Rev. B** 70(23): 233408/1-233408/4.

Molnar, A., I. Bucsi, M. Bartok, G. Resofszki and G. Gati. 1991. Characterisation of acid-base properties of oxides via the selective ring-opening of 2-methyloxirane. **J. Catal.** 129: 303-306.

Morita, Y., H. Matsumoto, T. Kiruma, F. Kato and M. Takayasu. 1973. Adsorptive and catalytic properties of lanthanum Y zeolite in the alkylation of benzene with ethylene. **Bull. Jpn. Pet. Inst.** 15(1): 37-44.

Nakajima, T., S. Kasamatsu and Y. Matsuo. 1996. Synthesis and characterization of fluorinated carbon nanotube. **Eur. J. Sol. State Inor.** 33(9): 831-840.

Namuangruk, S., P. Pantu and J. Limtrakul. 2004. Alkylation of benzene with ethylene over faujasite zeolite investigated by the ONIOM method. **J. Catal.** 225(2): 523-530.

_____, P. Pantu and J. Limtrakul. 2005. Investigation of ethylene dimerization over faujasite zeolite by the ONIOM method. **ChemPhysChem** 6(7): 1333-1339.

_____, P. Khongpracha, P. Pantu and J. Limtrakul. 2006a. Structures and Reaction Mechanisms of Propene Oxide Isomerization on H-ZSM-5: An ONIOM Study. **J. Phys. Chem. B** 110(51): 25950-25957.

_____, P. Khongpracha, D. Tantanak and J. Limtrakul. 2006b. Application of ONIOM calculations to study the effect of the zeolite framework on the adsorption of alkenes to ZSM-5. **J. Mol. Catal. A** 256: 113-121.

_____, P. Khongpracha, Y. Tantirungrotechai and J. Limtrakul. 2007. Decomposition of nitrous oxide on carbon nanotubes. **J. Mol. Grap. Model.** 26(1): 179-186.

Nieminen, V., M. Sierka, D.Y. Murzin and J. Sauer. 2005. Stabilities of C3-C5 alkoxide species inside H-FER zeolite: A hybrid QM/MM study. **J. Catal.** 231(2): 393-404.

O'Connor, C.T. and M. Kojima. 1990. Alkene oligomerization. **Catal. Today** 6(3): 329-349.

Olson, D.H. and E. Dempsey. 1969. The crystal structure of the zeolite hydrogen faujasite. **J. Catal.** 13(2): 221-231.

Ouyang, M., J.L. Huang and C.M. Lieber. 2002. Fundamental electronic properties and applications of single-walled carbon nanotubes. **Acc. Chem. Res.** 35(12): 1018-1025.

Pabchanda, S., P. Pantu, D. Tantanak and J. Limtrakul. 2004. Structure and energetics of nitrous oxide and methane adsorption on the FE-ZSM-5 zeolite: Oniom and density functional studies. **Stud. Surf. Sci. Catal.** 154 B: 1844-1848.

Panjan, W. and J. Limtrakul. 2003. The influence of the framework on adsorption properties of ethylene/H-ZSM-5 system: An ONIOM study. **J. Mol. Struct.** 654(1-3): 35-45.

Pelmenschikov, A. and J. Leszczynski. 1999. Adsorption of 1,3,5-trinitrobenzene on the siloxane sites of clay minerals: Ab initio calculations of molecular models. **J. Phys. Chem. B** 103(33): 6886-6890.

Picozzi, S., S. Santucci, L. Lozzi, L. Valentini and B. Delley. 2004. Ozone adsorption on carbon nanotubes: The role of Stone-Wales defects. **J. Chem. Phys.** 120(15): 7147-7152.

Raksakoon, C. and J. Limtrakul. 2003. Adsorption of aromatic hydrocarbon onto H-ZSM-5 zeolite investigated by ONIOM study. **J. Mol. Struct.-THEOCHEM** 631: 147-156.

Rappe, A.K., C.J. Casewit, K.S. Colwell, W.A. Goddard Iii and W.M. Skiff. 1992. UFF, a full periodic table force field for molecular mechanics and molecular dynamics simulations. **J. Am. Chem. Soc.** 114(25): 10024-10035.

Reddy, K.S.N., B.S. Rao and V.P. Shiralkar. 1993. Alkylation of benzene with isopropanol over zeolite beta. **Appl. Catal. A** 95(1): 53-63.

Rigby, A. M., G.J. Kramer and R.A. Van Santen. 1997. Mechanisms of hydrocarbon conversion in zeolites: a quantum mechanical study. **J. Catal.** 170(1): 1-10.

Rozanska, X., R.A. Van Santen, F. Hutschka and J. Hafner. 2001. A periodic DFT study of intramolecular isomerization reactions of toluene and xylenes catalyzed by acidic mordenite. **J. Am. Chem. Soc.** 123(31): 7655-7667.

_____, T. Demuth, F. Hutschka, J. Hafner and R.A. Van Santen. 2002. A periodic structure density functional theory study of propylene chemisorption in acidic chabazite: Effect of zeolite structure relaxation. **J. Phys. Chem. B** 106(12): 3248-3254.

_____, R.A. Van Santen, T. Demuth, F. Hutschka, and J. Hafner. 2003. A Periodic DFT Study of Isobutene Chemisorption in Proton-Exchanged Zeolites: Dependence of Reactivity on the Zeolite Framework Structure. **J. Phys. Chem. B** 107(6): 1309-1315.

Ruthven, D.M. and M. Goddard. 1986. Sorption and diffusion of C aromatic hydrocarbons in faujasite type zeolites. I. Equlilbrium isotherms and separation factor. **Zeolites** 6(8): 275-282.

Sepa, J., C. Lee, R.J. Gorte, D. White, E. Kassab, E.M. Evleth, H. Jessri, M. Allavena. 1996. Carbonyl^{13}C Shielding Tensors and Heats of Adsorption of Acetone

Adsorbed in Silicalite and the 1:1 Stoichiometric Complex in H-ZSM-5. **J. Phys. Chem.** 100(47): 18515-18523.

Shim, M., J.H. Back, T. Ozel and K.-W. Kwon. 2005. Effects of oxygen on the electron transport properties of carbon nanotubes. Ultraviolet desorption and thermally induced processes. **Phys. Rev. B** 71(20): 205411/1-205411/9.

Siffert, S., L. Gaillard and B.L. Su. 2000. Alkylation of benzene by propene on a series of Beta zeolites: Toward a better understanding of the mechanisms. **J. Mol. Catal. A** 153(1-2): 267-279.

Smirniotis, P.G. and E. Ruckenstein. 1995. Alkylation of benzene or toluene with MeOH or C2H4 over ZSM-5 or beta zeolite: Effect of the zeolite pore openings and of the hydrocarbons involved on the mechanism of alkylation. **Ind. Eng. Chem. Res.** 34(5): 1517-1528.

Smith, J.G. 1984. Synthetically useful reactions of epoxides. **Synthesis**. 8: 629-656.

Solans-Monfort, X., J. Bertran, V. Branchadell and M. Sodupe. 2002. Keto-enol isomerization of acetaldehyde in HZSM5. A theoretical study using the ONIOM2 method. **J. Phys. Chem. B** 106(39): 10220-10226.

Spoto, G., S. Bordiga, G. Ricchiardi, D. Scarano, A. Zecchina and E. Borello. 1994. IR study of ethene and propene oligomerization on H-ZSM-5: hydrogen-bonded precursor formation, initiation and propagation mechanisms and structure of the entrapped oligomers. **J. Chem. Soc., Faraday Trans.** 90(18): 2827-2835.

Stephens, P.J., F.J. Devlin, C.F. Chabalowski and M.J. Frisch. 1994. Ab Initio calculation of vibrational absorption and circular dichroism spectra using density functional force fields. **J. Phys. Chem.** 98(45): 11623-11627.

Sternberg, M., L.A. Curtiss, D.M. Gruen, G. Kedziora, D.A. Horner, P.C. Redfern, and P. Zapol**.** 2006. Carbon Ad-Dimer Defects in Carbon Nanotubes. **Phys. Rev. Lett.** 96(075506): 1-5.

Stewart, J.J.P. 1989. Optimization of parameters for semiempirical methods: I. Method. **J. Compt. Chem.** 10: 209-220.

Stewart, J.J.P. 1989. Optimization of parameters for semiempirical methods: II. Appication. **J. Compt. Chem.** 10: 221-264.

Su, M.D. 2005. Theoretical study of addition reactions of heavy carbenes to carbon and boron nitride nanotubes. **J. Phys. Chem. B** 109(46): 21647-21657.

_____, H.Y. Liao, W.S. Chung and S.Y. Chu. 1999. Cycloadditions of 16-electron 1,3-dipoles with ethylene. A density functional and CCSD(T) study. **J. Org. Chem.** 64(18): 6710-6716.

Svelle, S., S. Kolboe and O. Swang. 2004. Theoretical investigation of the dimerization of linear alkenes catalyzed by acidic zeolites. **J. Phys. Chem. B** 108(9): 2953-2962.

Svensson, M., S. Humbel, R.D.J. Froese, T. Matsubara, S. Sieber and K. Morokuma. 1996. ONIOM: A multilayered integrated MO + MM method for geometry optimizations and single point energy predictions. A test for Diels-Alder reactions and Pt(P(t-Bu)3)2 + H2 oxidative addition. **J. Phys. Chem.** 100(50): 19357-19363.

Szabo, A. and N.S. Ostlund. 1996. Modern Quantum Chemistry: Introduction to Advanced Electronic Structure Theory. **Dover Publication, Inc**., New York.

Tagmatarchis, N. and M. Prato. 2004. Functionalization of carbon nanotubes via 1,3-dipolar cycloadditions. **J. Mater. Chem.** 14(4): 437-439.

Treesukol, P., J.P. Lewis, J. Limtrakul and T.N. Truong. 2001. A full quantum embedded cluster study of proton siting in chabazite. **Chem. Phys. Lett.** 350(1-2): 128-134.

Triantafyllidis, K.S., A.A. Lappas, I.A. Vasalos, Y. Liu, H. Wang and T.J. Pinnavaia. 2006. Gas-oil cracking activity of hydrothermally stable aluminosilicate mesostructures (MSU-S) assembled from zeolite seeds: Effect of the type of framework structure and porosity. **Catal. Today** 112(1-4): 33-36.

Van Den Berg, J.P., J.P. Wolthuizen, A.D.H. Clague, G.R. Hays, R. Huis and J.H.C. Van Hooff. 1983. Low-temperature oligomerization of small olefins on zeolite H-ZSM-5. An investigation with high-resolution solid-state C NMR13. **J. Catal.** 80: 130-138.

Venuto, P.B., L.A. Hamilton and P.S. Landis. 1966. Organic reactions catalyzed by crystalline aluminosilicates: II. Alkylation reactions: Mechanistic and aging considerations. **J. Catal.** 5(5): 484-493.

_____ and P.S. Landis. 1968. Organic catalysis over crystalline aluminosilicates. **Adv. Catal.** 18: 259-371.

Vos, A.M., X. Rozanska, R.A. Schoonheydt, R.A. Van Santen, F. Hutschka and J. Hafner. 2001. A theoretical study of the alkylation reaction of toluene with methanol catalyzed by acidic mordenite. **J. Am. Chem. Soc.** 123(12): 2799-2809.

_____, R.A. Schoonheydt, F. De Proft and P. Geerlings. 2003. Reactivity descriptors and rate constants for acid zeolite catalyzed ethylation and isopropylation of benzene. **J. Phys. Chem. B** 107(9): 2001-2008.

Wang, C., G. Zhou, H. Liu, J. Wu, Y. Qiu, B.L. Gu and W. Duan. 2006. Chemical functionalization of carbon nanotubes by carboxyl groups on stone-wales defects: A density functional theory study. **J. Phys. Chem. B** 110(21): 10266-10271.

Warakulwit, C., S. Bamrungsap, P. Luksirikul, P. Khongpracha and J. Limtrakul. 2005. Diels-Alder cycloadditions of single-wall carbon nanotubes with electron-rich dienes: A theoretical study. **Stud. Surf. Sci. Catal.** 156: 823-828.

Weitkamp, J. 1985. Alkylation of hydrocarbons with zeolite catalysts-commercial applications and mechanistic aspects. **Acta Phys. Chem.** 31(1-2) 271-290.

Wesolowski, T.A., O. Parisel, Y. Ellinger and J. Weber. 1997. Comparative study of benzene-X (X = O_2, N_2, CO) complexes using density functional theory: The importance of an accurate exchange-correlation energy density at high reduced density gradients. **J. Phys. Chem. A** 101(42): 7818-7825.

Wu, X., J. Yang, J.G. Hou and Q. Zhu. 2006. Defects-enhanced dissociation of H_2 on boron nitride nanotubes. **J. Chem. Phys.** 124(5): 054706/1-054706/5.

Yamada, K., S. Kondo and K. Segawa. 2000. Selective catalytic reduction of nitrous oxide over Fe-ZSM-5: The effect of ion-exchange level. **Micropor. Mesopor. Mat.** 35-36: 227-234.

Yamada, K., C. Pophal and K. Segawa. 1998. Selective catalytic reduction of N2O by C_3H_6 over Fe-ZSM-5. **Micropor. Mesopor. Mat.** 21(4-6): 549-555.

Yim, W.L. and Z.F. Liu. 2004. A reexamination of the chemisorption and desorption of ozone on the exterior of a (5,5) single-walled carbon nanotube. **Chem. Phys. Lett.** 398(4-6): 297-303.

Zhang, L., J. Yang, C.L. Edwards, L.B. Alemany, V.N. Khabashesku and A.R. Barron. 2005. Diels-Alder addition to fluorinated single walled carbon nanotubes. **Chem. Commun.** 26: 3265-3267.

Zhou, L.G. and S.Q. Shi. 2003. Formation energy of Stone-Wales defects in carbon nanotubes. **Appl. Phys. Lett.** 83(6): 1222-1224.